Influence of the symmetry on the circular dichroism in angular resolved core–level photoemission

ARTICLE *in* JOURNAL OF ELECTRON SPECTROSCOPY AND RELATED PHENOMENA · FEBRUARY 2002

Impact Factor: 1.44 · DOI: 10.1016/S0368-2048(01)00355-3

ELSEVIER

Journal of Electron Spectroscopy and Related Phenomena 122 (2002) 157–180

JOURNAL OF ELECTRON SPECTROSCOPY and Related Phenomena

www.elsevier.com/locate/elspec

Influence of the symmetry on the circular dichroism in angular resolved core-level photoemission

G.H. Fecher[a,*], V.V. Kuznetsov[b], N.A. Cherepkov[b], G. Schönhense[a]

[a] *Johannes Gutenberg-Universität, Institut für Physik, D-55099 Mainz, Germany*
[b] *State University of Aerospace Instrumentation, 190000 St. Petersburg, Russia*

Received 7 June 2001; received in revised form 19 September 2001; accepted 19 September 2001

Abstract

The model for angular resolved photoemission from adsorbed atoms is extended to account for the non-axial symmetry of atoms in a crystal field. In particular, circular dichroism in the angular distribution (CDAD) is theoretically investigated. A special emphasis is put on the case when incident photons are propagating along the principal axis of an atom in C_{nv} symmetry. The model, although mainly developed for adsorbates, may also be used as a base for emission from solid surfaces. An extension to simple bulk symmetries, like D_{6h} for hexagonal or O_h for cubic crystals, is included. The CDAD for normal incidence does not vanish in the extended model and reflects the symmetry of the adsorption site. Scattering induced final state effects are discussed for alkali metal adsorption. A numerical calculation of the emission from the shallow 4p core level of Rb atoms adsorbed in a $(\sqrt{3}\times\sqrt{3})-R30°$ structure on a Pt(111) surface is presented. In this case even the extended photoemission model predicts the absence of CDAD. The appearance of CDAD is only possible due to the scattering of photoelectrons from the neighbouring atoms of the solid. © 2002 Published by Elsevier Science B.V.

Keywords: Photoemission; Dichroism; Symmetry; Adsorbates

PACS: 79.60; 61.50.A

1. Introduction

Angle and energy resolved photoemission from solids is a well-established tool for investigating the electronic and geometrical structure of solids, thin films and adsorbates. The use of high brilliance synchrotron radiation sources in combination with position sensitive detectors nowadays allows very fast three-dimensional photoelectron angular distributions with high resolution to be obtained [1,2]. They contain very rich information on the electronic and geometrical structure of targets. To disentangle this information, one needs to perform theoretical calculations capable of taking into account different aspects of the process. Two approaches are commonly used (for examples see [3,4]). One is based on the decomposition of the photoemission process into a sequence of simpler events, that are

(0) penetration of the photons through the surface and propagation in the solid;
(I) excitation of an electron;

*Corresponding author. Tel.: +49-6131-39-23631; fax: +49-6131-39-23807.
E-mail address: fecher@mail.uni-mainz.de (G.H. Fecher).

0368-2048/02/$ – see front matter
PII: S0368-2048(01)00355-3

(II) propagation of the electron to the surface;
(III) transmission of the electron through the surface into the vacuum.

Part (0) is connected to the properties of the photons and it is usually separated. The formalism using steps (I)–(III) separately is called the three-step model. In the case of core-level photoemission from adsorbates this model is often used in its two-step form, where (II) is mainly described by diffraction of the electrons by the atoms surrounding the emitter and (III) is omitted. Such models are successfully applied to core level photoemission (for examples see the reviewing articles by Fadley [2,5] or Woodruff and Bradshaw [6]). Usually they cannot be applied easily to emission from valence bands.

In the latter case the one-step models based on Pendry's work [7] considering steps (I)–(III) as a single event will give the best description [3,4]. These one-step models include the complete symmetry of the solid if using so-called full-potential methods and in their present form they are fully relativistic. In principle, the one-step model may also be used to describe core-level photoemission. Unfortunately, it is difficult to single out from these calculations what was the origin the of that or another effect. For example, was it of atomic origin or did it appear due only to the crystalline structure? Moreover, it is hard to include atomic many-body effects that manifest themselves in intershell interaction or in resonant processes into such type of calculation. Just these effects, as observed often in experiments (for examples see [8]), may be included very easily in step (I) of the many-step models. As starting point, most of the many-step photoemission calculations usually use relatively simple basic approximations for the atomic initial state wave functions and therefore do not always give satisfactory results.

Atomic models as proposed, for example in [9–11], have been used to explain different effects in photoemission from solids. But per se, such pure atomic models may fail to describe the angular distributions in photoemission from solids and surfaces as observed in experiments (for an example see Figs. 1 and 2 in [12]). This fact is indeed not surprising, because the geometrical structure of the solid is not taken into account in the free atom models. The scattering at the surrounding atoms will change the angular distributions drastically, as was first shown by Liebsch [13]. However, the atomic model may give an estimate of the general trend and the order of magnitude of some effects.

The atomic models, as formerly exploited, implied most often that polarised atoms are axially symmetric. This is usually the case in experiments with gas phase atoms. In a solid environment, one also has to consider that the atoms do not have an axial symmetry. The atomic model extended in that way has a broader applicability as an initial step for consideration of photoemission from solids and adsorbed atoms. To explain the differences with previous work, we will discuss mainly the influence of the solid state environment on the initial state of the target, while in a first approximation the final state in step (I) remains the same as in spherically symmetric atoms. The basic idea about using symmetry adapted wave functions was given by Gadzuk [14], Herbst [15] and Goldberg et al. [16]. Common to most previous works is that only symmetry adapted angular parts are used, often restricted to a cubic symmetry. We already used symmetry adapted angular parts in earlier work to describe dichroic effects in angular resolved photoemission experiments from adsorbates and clean surfaces [17,18]. However, these experiments were performed for off-normal photon incidence.

A well-known effect in photoemission is the circular dichroism in the angular distribution (CDAD) as it was termed in [19]. It was first mentioned by Feder [20] that a large difference in the differential cross-section appears in emission from adsorbates if the helicity of the exciting radiation is changed. Then it was shown that photoemission from polarised atoms [21] and from oriented (fixed-in-space) molecules [22,23] leads to the appearance of CDAD in the electric dipole approximation. The CDAD from solids appears due to the scattering induced final state interference in the case of spherical symmetry in the initial state as was discussed in [24]. So, in all cases the CDAD is the result of breaking the spherical symmetry of the system.

Today there is a large spectrum of models that are used to describe the CDAD from atoms being polarised (aligned or oriented) where the solid

environment is neglected (the usual atomic model of photoemission) [9–11,21,25–27]. Most often these models are only capable of describing a magnetic dichroism but not a circular dichroism from non-ferromagnetic solids. Thole and van der Laan also included symmetry considerations in their work [11] which is mainly about magnetic effects. In core-level emission from solids, the initial state is usually assumed to be spherically symmetric and CDAD appears solely due to scattering of photoelectrons from the surrounding atoms [13,24,28–35]. This applies also to cylindrically symmetric atoms and photon incidence along the symmetry axis. We will give an extended photoemission model of the CDAD including symmetry adapted initial state wave functions that may be used as a starting point for calculations describing photoemission from solid surfaces and adsorbed atoms in three-step calculations.

Some basic geometrical ideas will be recalled to find out what symmetries are most useful if investigating photoemission from adsorbates. In Fig. 1 we present different adsorption sites with local C_{iv} symmetry for low *hkl* indexed surfaces covering the most common crystalline structures of elemental metals. For the hexagonal surfaces one has to account for the stacking order of the hexagonally ordered planes that are ABC for fcc(111) and AB (hcp) or ABAC (dhcp) for hex(0001). B and C represent planes that are shifted differently with respect to the top most plane (A) shown in Fig. 1. This leads to a 3-fold rotational axis for fcc(111) surfaces and to a 6-fold screw axis for hcp(0001).

It is seen from Fig. 1 that the local C_{4v} or C_{6v} symmetries may be realised by adsorption on a single site. The bridge sites with local C_{2v} or C_{3v} symmetries are not connected unambiguously to a single site in most cases, but only hollow or on top sites with C_{2v} on the bcc(110) surface (for the cases given here). The case of the C_{3v} site will be discussed below in detail. In general, it will be found that one will observe an average of the photoemission intensities from sites with different orientation of the local environment, independent of whether one has an ordered or a random distribution of the adsorbed atoms at the surface. The ordered phases will result in domains that are possibly resolved in experiments, but then one has to account for the symmetry implied by the neighbouring adsorbate atoms, too. The result, what symmetry will dominate, will depend whether the interaction with the substrate or the neighbouring adsorbate atoms is stronger.

In a general case, the angular distributions are

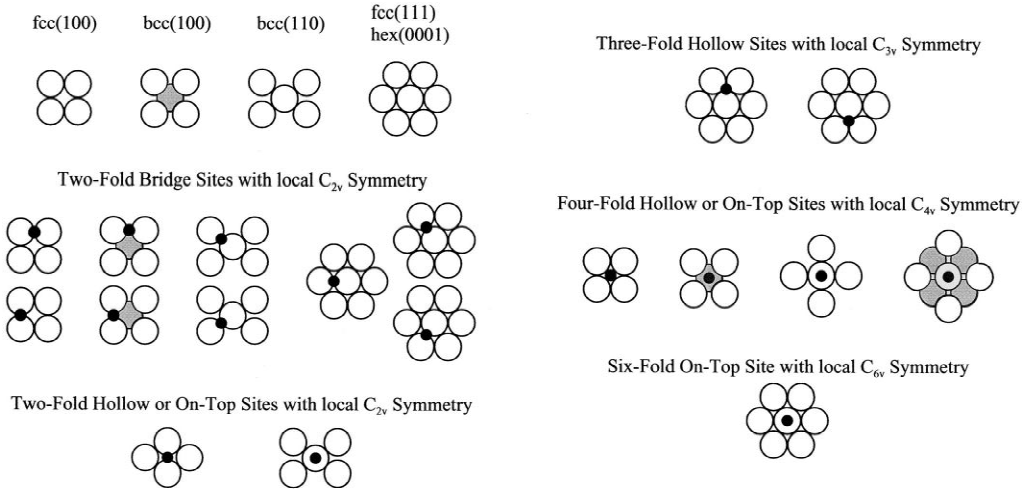

Fig. 1. Adsorption sites on low indexed surfaces of the most common crystalline structures of elemental metals and their local symmetry. Grey drawn atoms are located in the subsurface plane. Several adsorption sites may be realised in different ways, in these cases an average will lead virtually to a different symmetry (for an example see Fig. 3). Note that only the local symmetry is shown, the global symmetry may differ for particular structures.

described by very lengthy expressions and therefore we restrict the discussion in this paper to the CDAD. The CDAD for aligned states considered is a pure interference effect and therefore contains fewer terms than the total cross section. It follows from the atomic model that the CDAD vanishes in a spherical environment, therefore it can easily be used to show where the differences between the standard and the extended atomic models are. It is worthwhile to note that the CDAD investigated in the present work is not a magnetic or ferromagnetic effect. It is not connected to an orientation of the atoms but only to their alignment.

The paper is organised as follows. In Section 2, we introduce the formalism for symmetry adapted initial state wave functions and define the CDAD. The implications of the symmetry adapted wave functions on the CDAD are discussed in Section 3 and applied to atoms belonging to the C_{2v} symmetry group. Sections 4–7 are devoted to the consideration of the CDAD for the C_{3v}, C_{4v} and C_{6v} symmetry groups as well as some groups for bulk photoemission (O_h, $D_{6\ h}$). Section 8 is about the effect of the symmetry on the final state. Section 9 remarks on the coupling of states induced by the crystal field potential. Section 10 is devoted to the states of the double groups. Finally, we discuss in Section 11 adsorbates on substrates having C_{3v} and C_{6v} symmetry where the atomic model is unable to describe adequately the CDAD from p-shells. The results of numerical calculations of CDAD for different adsorption sites are presented which include the photoelectron diffraction in a cluster description.

2. General expression for the angular distribution and CDAD

In previous considerations of photoionization of polarised atoms [27,36] it was implied that an ensemble of atoms polarised in some direction $\boldsymbol{n}$ is axially symmetric. In other words, this ensemble is described by a diagonal density matrix in the coordinate frame with the z axis directed along $\boldsymbol{n}$. Atoms in crystals and atoms adsorbed on surfaces do not always possess an axial symmetry, and therefore must be described by a nondiagonal density matrix in any coordinate frame. The angular distribution $I^{j}(\boldsymbol{k},\boldsymbol{n})$, as derived for example in [37] for the case of axially symmetric polarised atoms, has to be corrected in order to account for the nondiagonal density matrix $p^{\boldsymbol{n}}_{NM_{N'}}$. This leads to the following equation for the case of the lower (non-axial) symmetry

$$I^{j}(\boldsymbol{k},\boldsymbol{n}) = \frac{c_\sigma}{[l]}\sqrt{\frac{3[j]}{4\pi}}\sum_{\kappa,L}\sum_{N}[N]^{1/2}C^{j}_{\kappa LN}\sum_{x,M}\sum_{M_N,M'_N}\rho^{\gamma}_{\kappa x}\rho^{\boldsymbol{n}}_{NM_{N'}} (j)Y^{*}_{LM}(\boldsymbol{k})D^{N}_{M_N M_{N'}}(\Omega)\begin{pmatrix}\kappa & L & N\\ x & M & M_N\end{pmatrix} \quad (1)$$

l and j are the orbital and the total angular momentum of an electron in the initial state. C^{j}_{kLN} are the dynamic parameters and $\rho^{\gamma}_{\kappa x}$ are the photon state multipoles [38]. $D^{j}_{mm_j}(\Omega)$ is the Wigner rotation matrix with Ω being the set of Euler angles describing the rotation from the laboratory to the atomic coordinate frame. The direction of the electron momentum $\boldsymbol{k}$ is defined by the angles θ and ϕ (see Fig. 2). Finally, c_σ is a photon energy (ω) dependent constant (α is the fine structure constant)

$$c_\sigma = \frac{4\pi^2 a\omega}{3} \quad (2)$$

The formalism can also be used to consider open shell atoms. In that case, the dynamic parameters $C^{j}_{\kappa LN}$ have to be calculated for the appropriate coupling scheme (*jj*, *LS* or intermediate) with the single particle quantum numbers j,m being replaced by those (J,M) describing the complete atomic state [37]. However, this will not change the basic principles behind the model used here. The dynamic parameter will merely distribute the single-electron results in a particular way over the states of a multiplet (see [11,39]).

One finds from Eq. (1) that the CDAD vanishes for normal incident photons and any ensemble of axially symmetric aligned atoms [37], while it is different from zero even for $\boldsymbol{q}\|-\boldsymbol{n}$ for atoms in a reduced symmetry (for example C_{nv} or O_h). In the following it is always assumed that $\boldsymbol{n}//z$ is the outward directed surface normal and that at least one of the axes (x or y) corresponds to a symmetry plane (see Fig. 2).

As Eq. (1) leads to rather complicated equations in

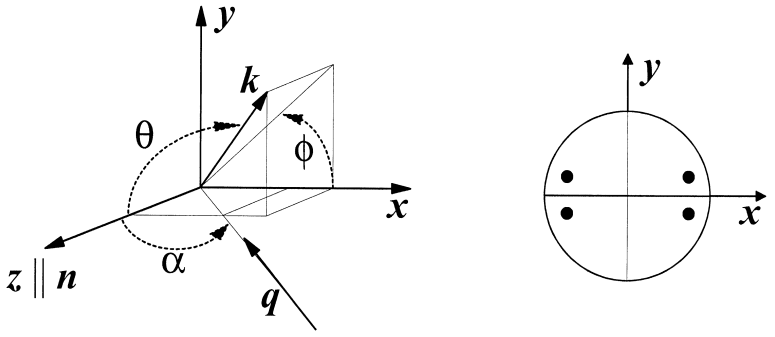

Fig. 2. Sketch of the $(\sqrt{3}\times\sqrt{3})-R30°$ structure realised on different adsorption sites of a hexagonal surface. In case of a fcc(111) surface one also has to account for the different stacking order ABC or ACB of the hexagonal planes of the substrate. In one 3-fold hollow domain all adsorbate atoms occupy up-triangle-oriented- and in the other domain down-triangle-oriented hollows. The incoherent superposition of these two domains with locally different orientation of the 3-fold hollow site results in a quasi or pseudo 6-fold symmetry. (The adsorbate and substrate atoms are not drawn to scale).

the most general case, we will restrict ourselves here to the single electron description. We start by calculating the photoemission cross section from Fermi's golden rule [16,40]. The photoelectron intensity for a transition from a bound initial state $\Psi_i = \Psi_{n,l,j}$ to a free photoelectron final state $\Psi_f = \Psi_{E_{\mathrm{kin}},\vec{k}}$ is given in the dipole length form by

$$\begin{aligned} I(\vartheta,\varphi) &= c_\sigma |\vec{\varepsilon}\cdot\langle\Psi_f|\vec{r}|\Psi_i\rangle|^2 \\ &= c_\sigma |\vec{\varepsilon}\cdot\vec{\xi}|^2 = c_\sigma |\varepsilon_x\xi_x + \varepsilon_y\xi_y + \varepsilon_z\xi_z|^2 \end{aligned} \tag{3}$$

$\vec{\varepsilon}\cdot\vec{r}$ is the dipole-operator with the unit polarisation vector $\vec{\varepsilon}$ and c_σ was already defined in Eq. (2). The polarisation vector does not depend on the integration variables and therefore it is separated from the transition matrix-element. Finally, it is seen that the photoelectron cross-section can be described using products from the components of the polarisation vector, where ε_i are the real (x,z) and complex (y) components of the polarisation vector. The transition matrix-element is separated in a vector whose components are excited by the corresponding parts of the position vector. $\xi_i(\theta,\phi)$ are complex matrix elements describing the photoelectron amplitude and therefore the angular distribution of the emitted photoelectrons.

Now, we simplify Eq. (3) for circularly polarised light by taking only the y component of the polarisation vector as complex and assuming the x and z components to be real. The matrix element describing the angular dependent amplitude of the outgoing photoelectron is given by (neglecting all pre-factors)

$$M_{f,i} = \vec{\varepsilon}\cdot\vec{\xi} = \begin{pmatrix} \varepsilon_x \\ \pm i\cdot\varepsilon_{yi} \\ \varepsilon_z \end{pmatrix} \cdot \begin{pmatrix} \xi_{xr} + i\cdot\xi_{xi} \\ \xi_{yr} + i\cdot\xi_{yi} \\ \xi_{zr} + i\cdot\xi_{zi} \end{pmatrix} \tag{4}$$

The photoelectron current is proportional to the square absolute of the matrix element $I = c_\sigma |M_{f,i}|^2$. The CDAD, that is the difference of the intensity for opposite helicity, may now simply be found by switching the sign of the y component from

$$\begin{aligned} I_{\mathrm{CDAD}} &= I^{i+} - I^{i-} \\ &= 2\cdot c_\sigma\cdot\varepsilon_{yi}\cdot\{2\cdot\varepsilon_x\cdot\mathcal{T}(\xi_x\xi_y^*) + 2\cdot\varepsilon_z\cdot\mathcal{T}(\xi_y^*\xi_z)\} \end{aligned} \tag{5}$$

($\mathcal{T}$ assigns the imaginary part).

Note that none of the results derived in this work changes if we assume elliptically polarised light where the y component has an additional real part: $\varepsilon_y = \varepsilon_{yr} \pm i\cdot\varepsilon_{yi}$, at least if only the helicity of the photons is changed but not the orientation of the polarisation ellipsis. In that case Eq. (5) becomes dependent on the degree of circular polarisation.

The components of the photon polarisation vector depend on the direction of propagation (see Fig. 2). For simplicity, we assume that the photon incidence is in the $\boldsymbol{x}-\boldsymbol{z}$ plane where one has for completely circularly polarised light

$$\vec{\varepsilon} = \sqrt{1/2}\begin{Bmatrix}\cos(\vartheta_q)\\ \pm i\\ -\sin(\vartheta_q)\end{Bmatrix} \tag{6}$$

Here, $\vartheta_q = \alpha + \pi$ gives the photon propagation measured with respect to the surface normal $\boldsymbol{n}$ and α is the angle of incidence as defined in optics. However, all other cases of photon incidence may be found by using appropriate rotations. It is easily seen from Eqs. (5) and (6) that the CDAD is given by a superposition of a normal incidence ($\alpha = 0$) and a grazing incidence ($\alpha = \pi/2$) term

$$\begin{aligned} I_{\mathrm{CDAD}} &= -2\cdot c_\sigma\cdot\{\cos(a)\cdot\Im(\xi_x\xi_y^*) - \sin(a)\cdot\Im(\xi_y^*\xi_z)\}\\ &= \cos(a)\cdot I_{\mathrm{CDAD}}^{\mathrm{NI}} + \sin(a)\cdot I_{\mathrm{CDAD}}^{\mathrm{GI}} \end{aligned} \tag{5a}$$

This has the advantage that we are able to investigate both types of CDAD, independently of each other. Both contributions may be separated from measurements taken at two different angles of photon incidence (note that $\alpha = \pi/2$ is not applicable at a surface). As already mentioned, the CDAD of the atomic model for axially aligned atoms vanishes if $\alpha = 0$ and therefore we will concentrate in this work mainly on the first term to study the influence of the symmetry on the CDAD. We will abbreviate this term to NI-CDAD.

In order to find the CDAD, we have finally to calculate the polarisation resolved matrix elements $\xi_{x,y,z}$ from

$$\begin{aligned} \xi_{x,y,z} &= \sum_{f,i} \langle\psi_f|e_{x,y,z}|\psi_i\rangle\cdot\langle R_f|r|R_i\rangle\cdot\exp[i\delta_f]\\ &= \sum_{f,i} \psi_{fi}^{x,y,z}(\theta,\varphi)\cdot D_{fi}\exp[i\delta_f] \end{aligned} \tag{7}$$

The angular parts $\psi_{fi}^{x,y,z}$ are calculated from the unit components e_{i} of the position vector in x, y or z directions. The D_{fi} are the usual radial integrals. All matrix elements are calculated here for the initial (and final) states of appropriate symmetry as will be given in the following. The procedure used here is principally the same as that described in [16] but extended for use with circularly polarised light. The only parameters needed to calculate the first integral in Eq. (7) are the Gaunt-coefficients as tabulated by Condon and Shortley [41].

2.1. Symmetry adapted wave functions

In the present work, symmetry adapted spherical harmonics [41] of the appropriate symmetry group will be used to find the CDAD for an l subshell of atoms in a particular symmetry. The wave function of an l electron is constructed as a combination of symmetry adapted spherical harmonics (the angular part) and radial functions R. The allowed combinations may be found by means of the projector technique as described by Ludwig and Falter [42]: $\Psi_g = P_g^{\Omega} Y_{lm} R_{nl} = \Sigma_{n,l,m}\, a_{g,nlm}^{\Omega} Y_{lm} R_{nl}^{g}$. P is the projector of the symmetry group, g serves as symmetry index and Ω assigns the set of Euler angles describing the symmetry operations of the group. The spherical harmonics Y_{lm} have to be replaced by spinors Ω_{jm}^{l} to account for the states of the double groups.

The energy of the states and the radial functions R_{nl}^{g} are found by solving the Schrödinger (or Dirac) equation for the atom in the crystal field of a definite symmetry. The crystal field potential may be expressed as a series using spherical harmonics [42]: $V_{\mathrm{CF}} = V_0\ \Sigma_{k,n}\ b_{kn} Y_{kn} r^k$. V_0 gives the strength of the crystal field and the coefficients b_{kn} are chosen in such a way that V_{CF} belongs to the appropriate symmetry group. The even components of the crystal field acting on electrons with orbital angular momenta from s to f are summarised in Table 1 for the symmetries considered in this work.

The lowest order perturbational energy of the crystal field is given by: $E_{\mathrm{g}} = \langle\Psi_{\mathrm{g}}|V_{\mathrm{CF}}|\Psi_{\mathrm{g}}\rangle$. These additional energies will give rise to an energetical splitting of the unperturbed atomic states. As a result, states of different symmetry become distinguishable.

In general, the crystal field will mix not only states of different projection m but also those of different l, but spinors with different j but the same l are not directly coupled. This is a consequence of the crystal field that does not act on the spin. A convenient approximation is to take only the part of solutions of the wave equation that correspond to nl or nlj electrons. As a direct consequence, all symmetry adapted spinors stay axial symmetric and will therefore not contribute to the normal incidence CDAD. We will comment on that fact later.

Further, we make use of linear combinations of spherical harmonics Y_{lm_l} with the same l but different m_l that result in real functions. These are assigned to the Cartesian coordinates x, y, z, or combinations of those [43]. The symmetry adapted p, d and f initial

Table 1
Crystal field potential: the non-zero, even components of the crystal field acting on electrons with orbital angular momentum l from 0 to 3. The components are abbreviated as $v_{kn} = V_{kn} Y_{kn} r^k$, where V measures the strength of the potential component. For spinors, these components always act on the state with $j = l + 1/2$; note that there are also odd k components with V_{k0} present in C_{nv} symmetry. The V_{kn} of the O_h group depends on the type of the cubic crystal structure sc (O_h^1), bcc (O_h^5), or fcc (O_h^9)

V_{CF}		Angular momentum l, j			
		s $s_{1/2}$, $p_{1/2}$	p $p_{3/2}$, $d_{3/2,}$	d $d_{5/2}$, $f_{5/2}$	f $f_{7/2}$
Symmetry group	C_{2v}	v_{00}	$+v_{20}+v_{22}$	$+v_{40}+v_{42}+v_{44}$	$+v_{60}+v_{62}+v_{64}+v_{66}$
	C_{3v}	v_{00}	$+v_{20}$	$+v_{40}+v_{43}$	$+v_{60}+v_{63}+v_{66}$
	C_{4v}	v_{00}	$+v_{20}$	$+v_{40}+v_{44}$	$+v_{60}+v_{64}$
	C_{6v}	v_{00}	$+v_{20}$	$+v_{40}$	$+v_{60}+v_{66}$
	O_h	v_{00}	$+v_{20}$	$+v_{40}+v_{44}$	$+v_{60}+v_{64}$
	D_{6h}	v_{00}	$+v_{20}$	$+v_{40}$	$+v_{60}+v_{66}$

states are given in Tables 2–6 for some C_{nv} and the O_h symmetry groups. States given in the same row may be coupled by the crystal field. The e representations are usually complex and degenerate. The corresponding basic functions were orthogonalised by building the appropriate linear combinations of spherical harmonics that are real. Some states are pairwise degenerate and have the same projections, these are given in different rows and the same

Table 2
Symmetry adapted initial state wave functions for atoms in C_{2v} symmetry. The first column gives the Mullikan symbol, the second column the assignment in solid state notation, its indices are the number i and the lowest orbital angular momentum (s, p,d, f, g . . . =0,1,2,3,4 . . .) contributing to the state. (Here and in the following tables the subscript z^2 is used as a short for $3z^2 - r^2$ and z^3 is used as a short for $z(5z^2 - 3r^2)$. Similarly we use in this table x^2 for $3x^2 - r^2$ and y^2 for $3y^2 - r^2$)

C_{2v} States		$l=1$	$l=2$	$l=3$
a_1	Σ_{1s}	$p_z R_p^{a_1}$	$d_{x^2} R_d^{a_1}$; $d_{y^2} R_d^{a_1}$; $d_{z^2} R_d^{a_1}$	$f_{z^3} R_f^{a_1}$; $f_{z(x^2-y^2)} R_f^{a_1}$
a_2	Σ_{2d}	–	$d_{xy} R_d^{a_2}$	$f_{xyz} R_f^{a_2}$
b_1	Σ_{3p}	$p_x R_p^{b_1}$	$d_{xz} R_d^{b_1}$	$f_{xz^2} R_f^{b_1}$; $f_{x(x^2-3y^2)} R_f^{b_1}$
b_2	Σ_{4p}	$p_y R_p^{b_2}$	$d_{yz} R_d^{b_2}$	$f_{yz^2} R_f^{b_2}$; $f_{y(3x^2-y^2)} R_f^{b_2}$

Table 3
Symmetry adapted initial state wave functions for atoms in C_{3v} symmetry. (Degenerate states with the same projection are given in one column. States that may be coupled by the crystal field are given in one row. Other quantities as in Table 2)

C_{3v} States		$l=1$	$l=2$		$l=3$	
a_1	Λ_{1s}	$_pzR_p^{a_1}$	$d_{z^2} R_d^{a_1}$		$f_{z^3} R_f^{a_1}$; $f_{x(x^2-3y^2)} R_f^{a_1}$	
a_2	Λ_{2f}	–	–		$f_{y(3x^2-y^2)} R_f^{a_2}$	
e	Λ_{3p}	$p_x R_p^e$	$d_{xz} R_d^e$	$d_{xy} R_d^e$	$f_{xz^2} R_f^e$	$f_{xyz} R_f^e$
		$p_y R_p^e$	$d_{yz} R_d^e$	$d_{x^2-y^2} R_d^e$	$f_{yz^2} R_f^e$	$f_{z(x^2-y^2)} R_f^e$

Table 4
Symmetry adapted initial state wave functions for atoms in C_{4v} symmetry. (The first non-zero a_2 state appears for $l=4$. Other quantities as in Tables 2 and 3)

C_{4v} States		$l=1$	$l=2$	$l=3$	
a_1	Δ_{1s}	$p_z R_p^{a_1}$	$d_{z^2} R_d^{a_1}$	$f_{z^3} R_f^{a_1}$	
a_2	Δ_{2g}	–	–	–	
b_1	Δ_{3d}	–	$d_{x^2-y^2} R_d^{b_1}$	$f_{z(x^2-y^2)} R_f^{b_1}$	
b_2	Δ_{4d}	–	$d_{xy} R_d^{b_2}$	$f_{xyz} R_f^{b_2}$	
e	Δ_{5p}	$p_x R_p^e$	$d_{xz} R_d^e$	$f_{xz^2} R_f^e$	$f_{x(x^2-3y^2)} R_f^e$
		$p_y R_p^e$	$d_{yz} R_d^e$	$f_{yz^2} R_f^e$	$f_{y(3x^2-y^2)} R_f^e$

Table 5
Symmetry adapted initial state wave functions for atoms in C_{6v} symmetry. (The first non-zero a_2 state appears for $l=4$. Other quantities as in Tables 2 and 3)

C_{6v} States		$l=1$	$l=2$	$l=2$
a_1	Γ_{1s}	$p_z R_p^{a_1}$	$d_{z^2} R_d^{a_1}$	$f_{z^3} R_f^{a_1}$
a_2	Γ_{2g}	–	–	–
b_1	Γ_{3f}	–	–	$f_{x(x^2-3y^2)} R_f^{b_1}$
b_2	Γ_{4f}	–	–	$f_{y(3x^2-y^2)} R_f^{b_2}$
e_1	Γ_{6p}	$p_x R_p^{e_1}$	$d_{xz} R_d^{e_1}$	$f_{xz^2} R_f^{e_1}$
		$p_y R_p^{e_1}$	$d_{yz} R_d^{e_1}$	$f_{yz^2} R_f^{e_1}$
e_2	Γ_{5d}	–	$d_{x^2-y^2} R_d^{e_2}$	$f_{(x^2-y^2)z} R_f^{e_2}$
			$d_{xy} R_d^{e_2}$	$f_{xyz} R_f^{e_2}$

Table 6
Symmetry adapted initial state wave functions for atoms in O_h symmetry. (Representations that require $l>3$ are omitted. Other quantities as in Tables 2 and 3)

O_h States		$l=1$		$l=2$		$l=3$	
a_{1u}	Γ_{1s}	–		$d_{x^2}R_d^{a_{1u}}$; $d_{y^2}R_d^{a_{1u}}$; $d_{z^2}R_d^{a_{1u}}$		–	
a_{2u}	Γ_{2f}	–		–		$f_{xyz}R_f^{a_{2u}}$	
e_g	Γ_{3d}	–		$d_{z^2}R_d^{e_g}$	$d_{x^2-y^2}R_d^{e_g}$	–	
t_{1u}	Γ_{4p}	$p_xR_p^{t_{1u}}$ $p_yR_p^{t_{1u}}$	$p_zR_p^{t_{1u}}$	–		$f_{x^3}R_f^{t_{1u}}$; $f_{y^3}R_f^{t_{1u}}$; $f_{z^3}R_f^{t_{1u}}$	
t_{2g}	Γ_{5d}	–		$d_{xz}R_d^{t_{2g}}$ $d_{yz}R_d^{t_{2g}}$	$d_{xy}R_d^{t_{2g}}$	–	
t_{2u}	Γ_{5f}	–		–		$f_{x(x^2-3y^2)}R_f^{t_{2u}}$ $f_{y(3x^2-y^2)}R_f^{t_{2u}}$	$f_{(x^2-y^2)z}R_f^{t_{2u}}$

column. (Note that other authors may give such pairs in brackets, see e.g. [43]). Some triply degenerate states occur in the O_h symmetry group.

For example, the wave function for the totally symmetric state a_1 of a p electron in C_{2v} symmetry is defined by $\psi_{a_1}^p = Y_{10}R_p^{a_1}\chi_{1/2(m_s)} = p_zR_p^{a_1}\chi_{1/2(m_s)}$. p_z is the usual angular part of the z-aligned p electron wave function in the Cartesian notation (see e.g. [16]). $\chi_{1/2(m_s)}$ assigns the two possible directions of the electron spin with respect to the C_2 rotational axis. In Tables 2–6 the Kramers spin-degeneracy is omitted for simplification.

Table 7
CDAD from initial p states. All equations for the initial p electrons are divided by: $c_\sigma \cdot 4\pi \cdot r \sin(\delta)$, where the radial integrals and relative final state phases are abbreviated by: $r = D_{d,p} \cdot D_{s,p}$ and $\delta = \delta_d - \delta_s$, respectively

p state CDAD	Normal incidence ($\alpha = 0°,\ q \| - z$)	Grazing incidence ($\alpha = 90°,\ q \| - x$)
p_x	$-\sin^2(\theta)\sin(2\phi)$	0
p_y	$+\sin^2(\theta)\sin(2\phi)$	$-\sin(2\theta)\sin(\phi)$
p_z	0	$+\sin(2\theta)\sin(\phi)$

Tables 7 and 8 give the normal and grazing incidence parts of the CDAD for most of the real linear combinations with orbital angular momentum $l=1,2$. Only the normal incident part is given in Table 9 for $l=3$ states, because the equations for the off-normal parts become too lengthy. The CDAD for the states in the correct symmetry has to be found by comparing Tables 7–9 with Tables 2–6, which will be discussed in the following sections.

It should be noted that not all possible equations may be found directly from Tables 7–9, because we neglected all couplings. A coupling of states will result in symmetry adapted wave functions that are not described by a single but by a linear combination of real orbitals. We restrict ourselves to the case of real coupling coefficients and only two states, so that the symmetry adapted wave function is given by $\Psi_g = c_1\Psi_{g1} + c_2\Psi_{g2}$. Inserting this state into Eq. (5) shows that the CDAD of the coupled wave functions is given by

$$I^{CDAD} = c_1^2 \cdot I_1^{CDAD} + c_2^2 \cdot I_2^{CDAD} + 2 \cdot c_1c_2 \cdot I_{(1),(2)}^{CDAD} \tag{8}$$

Table 8
CDAD from initial d states. All equations for initial d electrons are divided by: $c_\sigma \cdot 3\pi \cdot r \sin(\delta)$, where the radial integrals and relative final state phases are abbreviated by $r = D_{f,d} \cdot D_{p,d}$ and $\delta = \delta_f - \delta_p$, respectively

d state CDAD	Normal incidence ($\alpha = 0°,\ q \| - z$)	Grazing incidence ($\alpha = 90°,\ q \| - x$)
d_{xy}	$-4 \cdot \sin^4(\theta) \cdot \sin(4\phi)$	$-2 \cdot \sin(2\theta)\sin^2(\theta) \cdot \sin(2\phi)\cos(\phi)$
d_{yz}	$-\sin^2(2\theta) \cdot \sin(2\phi)$	$+2 \cdot \sin(2\theta)\sin^2(\theta) \cdot \sin(2\phi)\cos(\phi)$
d_{z^2}	0	$-2 \cdot \sin(2\theta)[1-3\cos^2(\theta)] \cdot \sin(\phi)$
d_{yz}	$+\sin^2(2\theta) \cdot \sin(2\phi)$	$+2 \cdot \sin(2\theta)\{[1-3\cos^2(\theta)] - \sin^2(\theta) \cdot \cos)\} \cdot \sin(\phi)$
$d_{x^2-y^2}$	$+4 \cdot \sin^4(\theta) \cdot \sin(4\phi)$	$+2 \cdot \sin(2\theta)\sin^2(\theta) \cdot \sin(\phi)\cos(2\phi)$

Table 9
Normal incidence CDAD from initial f states. All equations for initial f electrons are divided by: $c_\sigma \cdot 3/2(\pi) \cdot r \sin(\delta)$, where the radial integrals and relative final state phases are abbreviated by $r = D_{g,f} \cdot D_{d,f}$ and $\delta = \delta_g - \delta_d$, respectively

f state CDAD	Normal incidence ($\alpha = 0°$, $q \| \| -z$)
$f_{x(x^2-3y^2)}$	$+5 \cdot [\cos^6(\theta) + 3\sin^2(\theta)\cos^2(\theta) - 1] \cdot \sin(6\phi)$
f_{xyz}	$+5 \cdot \sin^2(\theta)\sin^2(2\theta) \cdot \sin(4\phi)$
f_{xz^2}	$+[25\cos^6(\theta) - 35\cos^4(\theta) + 11\cos^2(\theta) - 1] \cdot \sin(2\phi)$
f_{z^3}	0
f_{yz^2}	$-[25\cos^6(\theta) - 35\cos^4(\theta) + 11\cos^2(\theta) - 1] \cdot \sin(2\phi)$
$f_{(x^2-y^2)z}$	$-5 \cdot \sin^2(\theta)\sin^2(2\theta) \cdot \sin(4\phi)$
$f_{y(3x^2-y^2)}$	$-5 \cdot [\cos^6(\theta) + 3\sin^2(\theta)\cos^2(\theta) - 1] \cdot \sin(6\phi)$

where

$$\frac{c_1 c_2}{c_\sigma} \cdot I^{\mathrm{CDAD}}_{(1),(2)} = -\cos(a) \cdot \mathcal{T}\{\xi_{1x}\xi^*_{2y} + \xi_{2x}\xi^*_{1y}\} + \sin(a) \cdot \mathcal{T}\{\xi^*_{1y}\xi_{2z} + \xi^*_{2y}\xi_{1z}\} \quad (8a)$$

Eq. (8) shows that the CDAD is given by the sum of the CDAD arising from the individual states and an additional, mixed term that has to be determined separately from the appropriate matrix elements. This mixed term does not couple terms arising from different photon incidence, so that we are still able to investigate the NI-CDAD separately. This does not change if we include more than two terms in Eq. (8). The dependence on the matrix elements becomes more complicated in Eq. (8a) if one of the coefficients is complex. Eq. (8) is also very helpful if some states are coupled for other reasons, as we will see later.

In all tables only the influence of the symmetry on the initial state is respected. The influence arising from the final state will be discussed later with reference to particular examples.

3. CDAD for atoms with C_{2v} symmetry

3.1. CDAD for the p subshell

Consider the CDAD for photoionization of a p subshell. It is suggested that the atom is adsorbed in a bridge site having usually C_{2v} symmetry, at least in the local environment, or that a p hole is formed in an atom belonging to a bcc(110) or a fcc(110) surface. According to Table 2, the a_1 state corresponds to a p_z orbital and the states b_1 and b_2 correspond to p_x and p_y orbitals, respectively. The p states are not longer energetically degenerate as in spherical or axially aligned atoms. The radial parts of the initial states and also the radial integrals are now different for the different representations. This is a direct consequence of the crystal field potential. As an example, the radial integrals for emission from the a_1 state (p_z) is given by

$$D^{a_1}_{s,p} = \langle R_s | r | R^{a_1}_{np} \rangle$$
$$D^{a_1}_{d,p} = \langle R_d | r | R^{a_1}_{np} \rangle \quad (9)$$

Here we assumed that the final state may still be approximated in spherical symmetry. Therefore, neither the final state radial functions R_s and R_d nor the final state phases δ_s and δ_d depend on the symmetry. We will comment on the effect of the symmetry on the final states later.

One finds immediately from Table 7 that the normal incidence CDAD (NI-CDAD) for the state a_1 is equal to zero in C_{2v} symmetry, whereas the grazing incidence CDAD is given by

$$I^{a_1}_{\mathrm{CDAD}}\left(a = \frac{\pi}{2}\right) \propto +\sin(2\theta)\sin(\phi) D^{a_1}_{s,p} D^{a_1}_{d,p} \sin(\delta_d - \delta_s) \quad (10)$$

The states b_1 and b_2 correspond to p_x and p_y orbitals, respectively. The CDAD in emission from these states is found from Table 7 to be given by

$$I^{b_1}_{\mathrm{CDAD}}(a=0) \propto -\sin^2(\theta)\sin(2\phi) D^{b_1}_{s,p} D^{b_1}_{d,p} \sin(\delta_d - \delta_s)$$
$$I^{b_2}_{\mathrm{CDAD}}(a=0) \propto +\sin^2(\theta)\sin(2\phi) D^{b_2}_{s,p} D^{b_2}_{d,p} \sin(\delta_d - \delta_s) \quad (11)$$

for normal incidence. For grazing incidence only the b_2 state will exhibit CDAD

$$I^{b_2}_{\mathrm{CDAD}}\left(a=\frac{\pi}{2}\right)\propto -\sin(2\theta)\sin(\phi)\cdot D^{b_2}_{\mathrm{s,p}}D^{b_2}_{\mathrm{d,p}}\sin(\delta_{\mathrm{d}}-\delta_{\mathrm{s}}) \quad (12)$$

The radial integrals D^g will be different in all cases because the states belong to different representations.

If the a_1, b_1 and b_2 states cannot be resolved in an experiment, then one will observe a superposition of the CDAD emerging from all states. As all radial integrals are different, one finds a remaining CDAD for normal as well as grazing incidence. This demonstrates clearly the deviation from the model for axially aligned atoms.

For example one finds the overall NI-CDAD for the p-states in C_{2v} symmetry by averaging the two terms in Eq. (11)

$$I^{b(p)}_{\mathrm{CDAD}}(a=0)\propto\sin^2(\theta)\sin(2\phi)\cdot [D^{b_2}_{\mathrm{s,p}}D^{b_2}_{\mathrm{d,p}}-D^{b_1}_{\mathrm{s,p}}D^{b_1}_{\mathrm{d,p}}]\sin(\delta_{\mathrm{d}}-\delta_{\mathrm{s}}). \quad (11a)$$

Indeed, it is expected to be small because the difference of the radial integrals is small, but it still has the same symmetry properties as the NI-CDAD from the individual states.

From Eqs. (11) and (13) it is seen that the normal incidence CDAD reflects the 2-fold symmetry of the C_{2v} site through the azimuthal sin (2ϕ) dependence. Therefore, we will concentrate on the normal incidence CDAD in the following.

3.2. CDAD for the d subshell

Consider the photoionization of a d subshell of an atom with C_{2v} symmetry. The wave functions corresponding to the a_1, a_2, b_1 and b_2 irreducible representations of the C_{2v} symmetry group are given in Table 2.

Using the equations given in Table 8, we find that the CDAD in the case of a d subshell differs from zero for all states of the C_{2v} symmetry group. The dependence of the NI-CDAD on the azimuthal angle ϕ differs for the a and b states. The a_1 state has three contributions, namely the d_{x^2}, d_{y^2} and d_{z^2} parts. The charge distribution of the d_{x^2} and d_{y^2} states has the same shape as a d_{z^2} orbital, but their major axis is aligned along the x or the y axis. However, all three orbitals transform independently like the a_1 representation of the C_{2v} group. The contribution from the d_{z^2} part to the NI-CDAD is zero and the CDAD for the state a_1 is defined, after averaging over the two remaining angular parts, by the equation

$$I^{a_1}_{CDAD}\propto +4\sin^4(\theta)\sin(4\phi)\cdot D^{a_1}_{\mathrm{p,d}}D^{a_1}_{\mathrm{f,d}}\sin(\delta_{\mathrm{f}}-\delta_{\mathrm{p}}) \quad (13a)$$

For the a_2 state we have:

$$I^{a_2}_{\mathrm{CDAD}}\propto -4\cdot\sin^4(\theta)\sin(4\phi)\cdot D^{a_1}_{\mathrm{p,d}}D^{a_1}_{\mathrm{f,d}}\sin(\delta_{\mathrm{f}}-\delta_{\mathrm{p}}) \quad (13b)$$

and for the b_1 and b_2 states the NI-CDAD is finally given by

$$I^{b_1}_{\mathrm{CDAD}}\propto -\sin^2(2\theta)\sin(2\phi)\cdot D^{b_1}_{\mathrm{p,d}}D^{b_1}_{\mathrm{f,d}}\sin(\delta_{\mathrm{f}}-\delta_{\mathrm{p}})$$
$$I^{b_2}_{\mathrm{CDAD}}\propto +\sin^2(2\theta)\sin(2\phi)\cdot D^{b_2}_{\mathrm{p,d}}D^{b_2}_{\mathrm{f,d}}\sin(\delta_{\mathrm{f}}-\delta_{\mathrm{p}}) \quad (13c)$$

The CDAD has an opposite sign for the irreducible representations a_1 and a_2, or b_1 and b_2. In principle, measuring the dependence of the CDAD on the azimuthal angle ϕ allows to distinguish the photoionization of the $a_{1,2}$ states [sin (4ϕ) oscillations in the CDAD] from the photoionization of the $b_{1,2}$ states [sin(2ϕ) oscillations in the CDAD].

4. CDAD for atoms with C_{3v} symmetry

Consider the case of photoionization of an atom with C_{3v} symmetry. It is suggested that either an atom is adsorbed on a fcc(111) or hcp(0001) surface in a 3-fold hollow site having C_{3v} symmetry, or that an atom of a clean fcc(111) surface is ionised. The wave functions of the one-electron p- to f-subshells are given in Table 3 for the C_{3v} symmetry group. Making calculations analogous to that for atoms with C_{2v} symmetry, we find that the NI-CDAD is equal to zero for all p and d states of the C_{3v} symmetry group. The a_1 state is axially symmetric for $l<3$ what causes the vanishing NI-CDAD. The degen-

eracy is responsible for the vanishing of the NI-CDAD from the e states with $l<3$.

The NI-CDAD of the a_1 f state is found from Table 9 to be

$$I^{a_1}_{\mathrm{CDAD}}(a=0)\propto +5\cdot P(\theta)\sin(6\phi)\cdot D^{a_1}_{d,f}D^{a_1}_{g,f}\sin(\delta_g-\delta_d)$$
with
$$P(\theta)=[\cos^6(\theta)+3\sin^2(\theta)\cos^2(\theta)-1] \quad (14)$$

For the a_2 state it has the same angular dependence but the opposite sign as well as different radial integrals. For the state e it is zero after averaging over all degenerate contributions.

The grazing incidence CDAD of the p to f states does not vanish even if the splitting of the states is not resolved. As in the case of C_{2v} symmetry, this is a consequence of the different radial integrals.

5. CDAD for atoms with C_{4v} symmetry

Consider the photoionization of an atom with C_{4v} symmetry. This corresponds either to the photoionization of an atom adsorbed in a 4-fold hollow adsorption site, or to the photoionization of an atom belonging to the (100) surface of a sc, fcc, or bcc substrate. The wave functions for different states of the p and d subshell in C_{4v} symmetry are given in Table 4. The normal incidence CDAD vanishes in emission from the p subshell, like in the case of C_{3v} symmetry.

The NI-CDAD differs from zero in case of the b_1 and b_2 states of the d subshell. From Table 8 we find that it is given by the equations

$$I^{b_1}_{\mathrm{CDAD}}(a=0)\propto +4\cdot\sin^4(\theta)\sin(4\phi)\cdot D^{b_1}_{p,d}D^{b_1}_{f,d}\sin(\delta_d-\delta_p)$$
$$I^{b_2}_{\mathrm{CDAD}}(a=0)\propto -4\cdot\sin^4(\theta)\sin(4\phi)\cdot D^{b_2}_{p,d}D^{b_2}_{f,d}\sin(\delta_d-\delta_p) \quad (15)$$

The CDAD is equal to zero for the states a_1 and e if $\boldsymbol{q}\|-\boldsymbol{n}$. This result is natural since the a_1 state is here axially symmetric. The CDAD for the degenerate states e has an opposite sign but the same magnitude, so that the sum results in a vanishing NI-CDAD. The NI-CDAD does not vanish even if the splitting of the b_1 and b_2 states is not resolved and it reflects the C_{4v} symmetry through the azimuthal oscillations.

6. CDAD from atoms with C_{6v} symmetry

The wave functions for different states of an atom in C_{6v} symmetry are given in Table 5 for p, d and f subshells. In our model, the NI-CDAD is equal to zero for all states of p and d subshells. For the a_1 state this result is due to the fact that it is axially symmetric. For the doubly degenerate states e_1 and e_2 the wave functions have the same form as those of an axially symmetric system. The summation over the degenerate states e_1 or e_2 gives the zero result.

From Table 9 it is directly seen that the NI-CDAD does not vanish for the b_1 and b_2 states of an initial f shell. In both cases it exhibits a $\sin^6(\theta)\sin(6\phi)$ angular dependence and reflects therefore the C_{6v} symmetry.

7. Remarks on atoms in O_h, d_{4h} and d_{6h} symmetry

The bulk atoms belong to the O_h group in case of cubic crystals. Strictly speaking, the Γ point of the Brillouin-zone (or alternatively in real space the centre of the Wigner–Seitz cell) of the cubic lattices belongs to the O_h point group. The symmetry adapted states are given in Table 6 for l up to 3. The p states belong in O_h symmetry to the threefold degenerate t_{1u} representation (p_x, p_y, p_z), so that no CDAD is expected independent of a particular direction of photon incidence. The d states belong to the representations a_{1g}, e_g (d_{z^2}, $d_{x^2-y^2}$) and t_{2g} (d_{xz}, d_{yz}, d_{xy}), where the latter two representations are 2- or 3-fold degenerate. Only the angular parts are given in brackets for simplicity. The CDAD vanishes for the a_{1g} states (note that $x^2+y^2+z^2=r^2$ is spherical symmetric) of the d shell for normal incidence (here one of the cubic axes), whereas it is non-zero for the degenerate e_g and t_{2g} states. In both cases its angular dependence is of the form $\sin^4(\theta)\sin(4\phi)$ and has an opposite sign for the two states.

The p states belong in D_{4h} symmetry to the a_{2u} (p_z) or the twofold degenerate e_u (p_x, p_y) representations [43], so that no NI-CDAD is expected. The d shell electrons belong to the a_{1g} (d_{z^2}), b_{1g} ($d_{x^2-y^2}$), b_{2g} (d_{xy}) and the doubly degenerate e_g (d_{xz}, d_{yz}) representations [43]. For $l=2$, only the b_{1g} and b_{2g} states exhibit a normal incidence CDAD that has the

same angular dependence as the compatible b_1 and b_2 states of the C_{4v} group. It vanishes for all other states.

On the basis of the results for some of the cubic groups, we conclude that the difference between the photoelectron intensities for left and right circularly polarised light observed in [44] for the d bands of Cu(100) and for the same geometry as considered here is mainly due to a CDAD. This holds also if more complete wave functions are used to describe the initial state, for example LCAO wave functions [45,46]. A small additional effect, being due to a spin-dependent surface transmission supposed in [44], cannot be excluded as its explanation is based on the same symmetry arguments. Indeed, there are no spin effects needed at all to explain the observation of CDAD, neither in the photoemission process nor in the scattering and refraction part as was first mentioned by Feder [20]. Anyway, it becomes even more probable that the observed effect was a pure CDAD due to the lower symmetry of the atoms in the surface plane and the sensitivity of UV photoemission to the surface.

In case of hexagonal crystals the bulk atoms may belong to the D_{6h} group. The p shell electrons belong in D_{6h} symmetry to the a_{2u} (p_z) or the 2-fold degenerate e_{1u} (p_x, p_y) representations. The d shell electrons belong to the representations a_{1g} (d_{z^2}), e_{1g} (d_{xz}, d_{yz}) and e_{2g} ($d_{x^2-y^2}$, d_{xy}), where the latter two representations are 2-fold degenerate. The normal incidence CDAD vanishes for all p and d shells but is non-zero for the b_{1u} and b_{2u} states of an f shell. This may be found from the symmetry properties and the compatibility relation of the states to those of the C_{6v} group [43].

8. CDAD induced by the final state symmetry (s and p subshells)

In the previous chapters we always assumed that the final states are independent of a particular symmetry. We did not mention the s states that belong to the a_1 representation for all symmetries given above. Applying the selection rule for the x and y component of the photons (normal incidence along z), we find that the final states in emission from s states are the p_x and p_y states. In case of the C_{2v} symmetry these states belong to two different representations (b_1 and b_2: see Table 2), whereas they belong to degenerate representations in all other cases of symmetry considered here. In the same way we find for the $a_1 - p_z$ state that the possible final states belong to different representations.

Now we assume that the final b_1 and b_2 states have different radial functions as well as different phases. This follows straightforwardly from the additional crystal field potential in the Schrödinger equation, that has to apply to the final state, too. The different radial parts will also cause different radial integrals D. The calculation of the CDAD for the a_1 ($l = 0,1$) states of the C_{2v} symmetry group results in

$$I^{a_1,s}_{\mathrm{CDAD}}(a=0) \propto \sin^2(\theta)\sin(2\phi)\cdot D^{a_1 b_1}_{\mathrm{s,p}} D^{a_1 b_2}_{\mathrm{s,p}} \sin(\delta_{\mathrm{p,b_1}} - \delta_{\mathrm{p,b_2}})$$
$$I^{a_1,p}_{\mathrm{CDAD}}(a=0) \propto \sin^2(2\theta)\sin(2\phi)\cdot D^{a_1 b_1}_{\mathrm{p,d}} D^{a_1 b_2}_{\mathrm{p,d}} \sin(\delta_{\mathrm{d,b_1}} - \delta_{\mathrm{d,b_2}}) \quad (16)$$

The dynamical parameters are now additionally assigned by the final state symmetry. Both states did not show a NI-CDAD if only the initial state symmetry is taken into account, but here it arises from the symmetry properties of the final state.

The same may apply to other states, too. There is no NI-CDAD in emission from the a_1 orbitals with $l = 0,1,2$ of the C_{3v}, C_{4v} and C_{6v} groups induced by the final state symmetry because the final states belong always to the same representations. Therefore, we analyse in a similar way the influence of the final state symmetry on the emission from the e states with $l = 1$ in C_{3v}, C_{4v} and C_{6v} symmetry. The NI-CDAD vanishes still for the e or e_1 states of the C_{3v} and C_{6v} symmetry groups. This result is clear because one needs at least $l = 3$ partial waves in the final state to observe a 3- or 6-fold symmetry. The NI-CDAD respecting final state symmetry does not vanish in the case of the C_{4v} group where it is given by

$$I^{e,p}_{\mathrm{CDAD}}(a=0) \propto \sin^4(\theta)\sin(4\phi)\cdot$$
$$D^{e,b_1}_{\mathrm{p,d}} D^{e,b_2}_{\mathrm{p,d}} \sin(\delta_{\mathrm{d,b_2}} - \delta_{\mathrm{d,b_1}}) \quad (17)$$

The azimuthal distribution of the NI-CDAD including final state symmetry is 2- or 4-fold for C_{2v} or C_{4v} and thus reflects the symmetry of the adsorption site. The magnitude of the CDAD depends mainly on

the final state phase difference between the two states with different representations. This difference will be small in most cases, and therefore the CDAD will also be small.

It is interesting to note that the CDAD always arises here ($l=0,1$) from the interference of partial waves with the same orbital angular momentum, in contrast to the CDAD induced by the initial state symmetry. Similar interference terms occur for initial states with $l=2$ or higher in addition to terms combining final state partial waves of different l.

Additional terms will also appear in cases of states that already exhibited CDAD as result of the initial state symmetry (see previous sections). However, these extra contributions may be small and do not change the principle symmetry properties of the observed CDAD.

9. Coupling of states by the crystal field

Next we investigate the coupling of the states caused by the crystal field. The crystal field of a C_{2v} adsorption site acting on the p electrons is given by (see Table 1)

$$V_{2v} = V_{00}Y_{00} + V_{10}Y_{10} + \{V_{20}Y_{20} \pm V_{22}[Y_{22} + Y_{2-2}]\} \quad (18)$$

The upper sign is for the case where a 2-fold bridge is aligned along the x axis, whereas the lower sign has to be used if the bridge is aligned along the y axis. The first term V_{00} merely shifts the energy of all states. The last two terms couple mainly states of the same l and m_l. The matrix elements $\langle p_g|Y_{2m}|p_g\rangle$ are different for all three p orbitals, which leads to different energies. However, there is no coupling between the three different orbitals. The middle term is the most interesting, because it couples states differing in l by 1. In particular it couples the p_x with d_{xz}, the p_y with d_{yz} and the p_z with s and d_{z^2} orbitals. The matrix elements of the p_z with s and d_{z^2} are usually stronger compared to the other ones and therefore we will concentrate on these.

The parity of a p_z orbital is opposite to that of s or d orbitals. The combination of such states leads therefore to a shift of the charge distribution, either towards the vacuum or towards the substrate, depending on the sign of the crystal field. This explains directly the occurrence of a dipole moment in adsorbed atoms as can be measured via changes in the work function during adsorption [47]. It was shown for adsorbed alkali atoms that the 5p semicore level of Cs on W also becomes polarised and not only the valence s electrons [48]. This type of coupling appears for all C_{nv} symmetry groups but vanishes for example in the case of the O_h bulk group where V_{k0} is identically zero for odd k.

We would now like to investigate the influence of this coupling on the CDAD. The a_1 states with zero projection are given in general by

$$\Psi_{a_1} = c_0 s R_s^{a_1} + c_1 p_z R_p^{a_1} + c_2 d_{z^2} R_d^{a_1} + \cdots \quad (19)$$

One finds that no additional terms will appear if analysing the normal incidence CDAD of this state via Eq. (8). But, it should be noted that the grazing incidence CDAD will be changed.

The equations for the other states of the C_{nv} symmetry groups will be similarly coupled and they are always given by a linear combination over all l values as in Eq. (19). The consequence for the NI-CDAD is that it will always exhibit the symmetry of the CDAD arising from the lowest contributing l. Therefore, the NI-CDAD has principally always the same symmetry as the C_{nv} adsorption site. Its complete angular dependence becomes much more complicated because we have to respect the mixed terms of Eq. (8), too. However, these extra terms do not affect the symmetry properties, as all initial states still belong to the same symmetry group and representation.

9.1. C_{3v} symmetry revisited

There was a worrying effect for atoms in C_{3v} symmetry, namely, we did not find a threefold pattern of the CDAD. The pattern became 6-fold for emission from f or d states if accounting in the second case for the final state symmetry. The cause was that we used the symmetry adapted initial states without allowing for any couplings. In particular the v_{43} term (see Table 1) will couple the d_{xz} and $d_{x^2-y^2}$ as well as the d_{yz} and d_{xy} orbitals. The corresponding initial state wave functions are given by linear combinations of the form

$$\Psi_{\mathrm{d}}^{1,2} = \frac{1}{\sqrt{2}}\left[\mathrm{d}_{xz}R_{1e}^{\mathrm{d}} \pm \mathrm{d}_{xy}R_{2e}^{\mathrm{d}}\right]$$
$$\Psi_{\mathrm{d}}^{3,4} = \frac{1}{\sqrt{2}}\left[\mathrm{d}_{yz}R_{1e}^{\mathrm{d}} \pm \mathrm{d}_{x^2-y^2}R_{2e}^{\mathrm{d}}\right] \quad . \tag{20}$$

(Note: positive signs belong to the states 1 and 3 and negative signs to states 2 and 4).

The hopping matrix elements $\langle\Psi_i|v_{43}|\Psi_j\rangle$ are equal for all allowed states and therefore all four coefficients are $|c| = 1/\sqrt{2}$. In addition, we find that at least the energies of the states 1 and 3 as well as 2 and 4 are pairwise equal. Analysing the CDAD for normal photon incidence we find the result

$$I_{\mathrm{CDAD}}^{e,d}(a=0) \propto \pm \sin(2\theta)\sin^2(\theta)\cos(3\phi)\cdot$$
$$D_{\mathrm{pd}}^{e}D_{\mathrm{pf}}^{e}\sin(\delta_{\mathrm{f}} - \delta_{\mathrm{p}}) \tag{21}$$

It is seen that one will observe the expected 3-fold symmetry of the NI-CDAD pattern after accounting for the correct coupling if there is an additional lifting of degeneracy and supposed it is resolved in an experiment.

10. CDAD in emission from the symmetry orbitals of double groups

The single group description is not longer valid, if the spin–orbit interaction is stronger than the crystal field. In that case, one has to use the symmetry orbitals of the double groups. The base functions are build from $|j,m_j\rangle$ spinors. Some symmetry adapted spinor spherical harmonics (mainly for the cubic groups) may be found in [49]. If needed, the coefficients c^g for all symmetry adapted spinors with total angular momentum up to $j=9/2$ may be calculated for 45 finite double point groups with the computer program published by Meyer et al. [50].

All symmetry adapted spinors exhibit an axial symmetry for the most common symmetries (C_{nv}) of adsorbed atoms as considered here. This means that the normal incidence CDAD vanishes for all those states. From this behaviour, one may conclude that the initial state symmetry will only be seen in CDAD measurements if the crystal field has a very much stronger influence than the spin–orbit interaction. In the last chapter we will see that the adsorbate symmetry is still seen from final state effects, even if this condition is not fulfilled. There are no additional terms for the CDAD arising from the final state (see Section 8) in the case of the double groups, at least for the geometry ($\boldsymbol{q}\|-\boldsymbol{n}$), states (s−f) and symmetries (C_{nv}, O_h) considered here. The absence of the NI-CDAD after inclusion of the spin needs some explanation. The cylindrical symmetry of all of the states is implied by the spin–orbit interaction and this leads to a loss of the other symmetry properties if no additional potential is introduced to the Hamiltonian. To overcome this problem we apply perturbation theory to the spinors using the crystal field potential. (Note that the result is the same if we apply the spin–orbit interaction as perturbation to the states of the single groups used in the previous sections.) We start with the even components as summarised in Table 1. A v_{10} component will appear for the C_{nv} symmetry groups. It mixes states of different l like $\mathrm{s}_{1/2}$ and $\mathrm{p}_{1/2}$. As in the case of the single groups, this will not induce any NI-CDAD. Therefore, we omit an investigation of this coupling but it should be kept in mind if investigating the CDAD for grazing incident photons or the intensities.

From the spherical symmetry of the $\mathrm{s}_{1/2}$ and $\mathrm{p}_{1/2}$ states, we find immediately that the v_{00} or v_{20} components will lead merely to an energy shift. Furthermore, the v_{22} component does not act on $\mathrm{p}_{1/2}$ states, so that no new effects on the CDAD will appear. In particular it will remain zero for those states, independent of the photon incidence or symmetry of the CF potential.

In general, the v_{k0} (k even) components act only on states with the same m_j and therefore they do not mix states but only shift their energy. The splitting of the states for different absolute values of m_j (lifting of the $|m_j|$ degeneracy) will result in a CDAD for grazing incidence. It will not induce any NI-CDAD because these energetically split states are still axially symmetric.

We have to search for non-vanishing v_{kn} (k even, $n \neq 0$) in order to find situations where states of different m_j are coupled by the crystal field. For $\mathrm{p}_{3/2}$ states this situation arises only in C_{2v} symmetry as seen from Table 1 (restricting to the symmetries dealt with in this work). For example, the substates $m_j = +3/2$ are coupled to the $m_j = -1/2$ substates

by the v_{22} component. The angular parts of the two coupled states are then given by

$$\begin{aligned} \mathrm{p}^1_{3/2} &= c_1 \mathrm{p}_{3/2\pm 3/2} + c_2 \mathrm{p}_{3/2,\mp 1/2} \\ \mathrm{p}^2_{3/2} &= c_2 \mathrm{p}_{3/2,\pm 3/2} - c_1 \mathrm{p}_{3/2,\mp 1/2} \end{aligned} \tag{22}$$

They are both doubly degenerate as indicated by the double sign for m_j. The coefficients $c_{1,2}$ depend on the strength of the crystal field. They may be calculated using standard perturbational methods as was already shown by Herbst [15].

The remaining part is to check if these states exhibit a NI-CDAD. Applying Eqs. (5) and (8) to the spinors and averaging over all degenerate components, we finally find the result

$$\begin{aligned} I^{1,\mathrm{p}_{3/2}}_{\mathrm{CDAD}}(a=0) &\propto -c_1 c_2 \frac{\sqrt{3}}{6} \sin^2(\theta) \sin(2\phi) D_{\mathrm{s,p}} D_{\mathrm{d,p}} \sin(\delta_\mathrm{d} - \delta_\mathrm{s}) \\ I^{2,\mathrm{p}_{3/2}}_{\mathrm{CDAD}}(a=0) &\propto c_1 c_2 \frac{\sqrt{3}}{6} \sin^2(\theta) \sin(2\phi) D_{\mathrm{s,p}} D_{\mathrm{d,p}} \sin(\delta_\mathrm{d} - \delta_\mathrm{s}) \end{aligned} \tag{23}$$

The spin–orbit interaction in the final state is omitted for simplicity because it does not change the angular dependence but only the dynamical parameters D and δ (see also below). It is seen that only the mixed term of Eq. (8) appears here.

The result is generally the same as found from the single group p states in C_{2v} symmetry. But the NI-CDAD depends now directly on the strength of the CF-potential and vanishes if the splitting of the states is not resolved in an experiment.

The v_{4n} components of the CF potential do not act on the $\mathrm{d}_{3/2}$ states and therefore the same situation as for the $\mathrm{p}_{3/2}$ state appears. A NI-CDAD of the $\mathrm{d}_{3/2}$ states occurs only in C_{2v} symmetry where it is given by

$$I^{1,2,\mathrm{d}_{3/2}}_{\mathrm{CDAD}}(a = 0) \propto \mp c_1 c_2 \frac{\sqrt{3}}{10} \sin^2(\theta) \sin(2\phi) D_{\mathrm{p,d}} D_{\mathrm{f,d}} \sin(\delta_\mathrm{f} - \delta_\mathrm{p}) \tag{24}$$

This shows that only the coupling coefficients and dynamical parameters differ from those of the $p_{3/2}$ state, whereas the angular distribution is the same.

Additional components of the CF potential will act on $d_{5/2}$ states (or higher). These components are different in C_{2v}, C_{3v}, or C_{4v} symmetry. In C_{6v} symmetry only the $|m_j|$ degeneracy is lifted. The C_{4v} crystal field mixes $m_j = 5/2$ with $m_j = -3/2$ substates. The C_{3v} crystal field mixes $m_j = 5/2$ with $m_j = -1/2$ substates. In both cases only two different types of substates are mixed, whereas the C_{2v} crystal field mixes $m_j = 5/2$ with $m_j = -3/2$ and $m_j = 1/2$ substates. As we found the NI-CDAD in C_{2v} symmetry already for the $p_{3/2}$ and $d_{3/2}$ states, we will concentrate here on the C_{3v} and C_{4v} symmetries.

In C_{3v} symmetry one finds the following coupled $d_{5/2}$ states

$$\begin{aligned} \mathrm{d}^0_{5/2} &= \mathrm{d}_{5/2,\pm 3/2} \\ \mathrm{d}^1_{5/2} &= c_1 \mathrm{d}_{5/2,\pm 5/2} + i \cdot c_2 \mathrm{d}_{5/2,\mp 1/2} \\ \mathrm{d}^2_{5/2} &= c_2 \mathrm{d}_{5/2,\pm 5/2} - i \cdot c_1 \mathrm{d}_{5/2,\mp 1/2} \end{aligned} \tag{25}$$

leading to a NI-CDAD that is given by

$$\begin{aligned} I^{0,\mathrm{d}_{5/2}}_{\mathrm{CDAD}}(a=0) &\equiv 0 \\ I^{1,2,\mathrm{d}_{5/2}}_{\mathrm{CDAD}}(a=0) &\propto \pm c_1 c_2 \frac{3\sqrt{10}}{20} \sin(2\theta) \sin^2(\theta) \cos(3\phi) \cdot D_{\mathrm{p,d}} D_{\mathrm{f,d}} \sin(\delta_\mathrm{f} - \delta_\mathrm{p}) \end{aligned} \tag{26}$$

In C_{4v} symmetry one has the following $d_{5/2}$ states

$$\begin{aligned} \mathrm{d}^0_{5/2} &= \mathrm{d}_{5/2,\pm 1/2} \\ \mathrm{d}^1_{5/2} &= c_1 \mathrm{d}_{5/2,\pm 5/2} + c_2 \mathrm{d}_{5/2,\mp 3/2} \\ \mathrm{d}^2_{5/2} &= c_2 \mathrm{d}_{5/2,\pm 5/2} - c_1 \mathrm{d}_{5/2,\mp 3/2} \end{aligned} \tag{27}$$

The energies and coupling parameter for the $\mathrm{d}_{5/2}$ states in C_{4v} symmetry were already given in the work of Herbst [15]. These states exhibit a NI-CDAD that is given by

$$\begin{aligned} I^{0,d_{5/2}}_{\mathrm{CDAD}}(a=0) &\equiv 0 \\ I^{1,2,\mathrm{d}_{5/2}}_{\mathrm{CDAD}}(a=0) &\propto \pm c_1 c_2 \frac{3\sqrt{5}}{20} \sin^4(\theta) \sin(4\phi) \cdot D_{\mathrm{p,d}} D_{\mathrm{f,d}} \sin(\delta_\mathrm{f} - \delta_\mathrm{p}) \end{aligned} \tag{28}$$

In all cases we observe the opposite sign for the CDAD from the coupled states and it always exhibits the same symmetry as the CF potential.

The $\mathrm{f}_{5/2}$ states behave in the same way as the $\mathrm{d}_{5/2}$ states and the only difference in the NI-CDAD are the differences in the coupling coefficients and the dynamical parameter. The $\mathrm{f}_{7/2}$ states may be treated

by the same approach. For most symmetries the equations will become very lengthy, therefore we omit a more detailed investigation. It should be noted that the NI-CDAD from the $f_{7/2}$ state in C_{6v} symmetry results in a 6-fold pattern, as was already found for the f states of the single groups.

Finally, we note that the NI-CDAD for the spinors of atoms belonging to the O_h or D_{6h} symmetry groups are found from the C_{4v} and C_{6v} groups, because the same even components of the CF potential appear (see Table 1).

11. Comparison of the C_{6v} and a pseudo-c_{6v} symmetry (p subshell)

We present below the results from two-step photoemission calculations for p states of adsorbed atoms, since even the extended atomic model gives zero CDAD for the C_{6v} symmetry group. We also examine how different adsorption sites can be distinguished from the azimuthal dependence of the CDAD. It is very often found for adsorbed atoms that there are domains with different symmetry of the adsorbates in the region being observed. Typical examples are the 3-fold hollow or 2-fold bridge sites on hexagonal surfaces (see Figs. 1 and 3). For example, two types of hollow sites may appear where each is of 3-fold symmetry. Due to the incoherent superposition of the contributions of these structures, one will detect a pattern with a quasi 6-fold symmetry. The main question is whether there is a way to distinguish from the observed CDAD pattern the superimposed 2- or 3-fold sites from the real 6-fold site, namely the on top site.

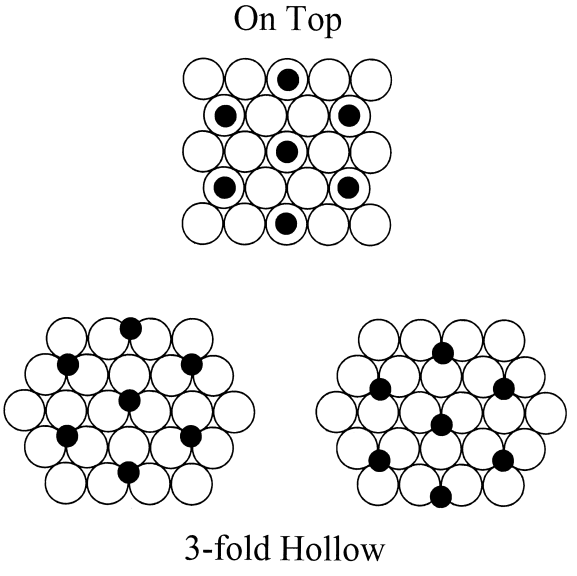

Fig. 3. Co-ordinate system used for the investigation of photoemission. k is the electron momentum, q is the photon beam and n is the principal axis of alignment. θ and ϕ are the angles defining the direction of the outgoing photoelectrons. α is the angle of photon incidence as defined in optics. The angle describing the photon propagation in spherical co-ordinates is given by $\vartheta_q = \alpha + \pi$. The direction of the z axis corresponds to n. The direction of the in-plane axes x and y is illustrated for an object with C_{2v} symmetry.

As an example we calculated the emission from the shallow p core level of alkali atoms adsorbed at a fcc(111) surface in the $(\sqrt{3}\times\sqrt{3})-R30°$ structure. The matter becomes complicated in that case for several reasons. From the geometrical point of view we have the possibility of either two different 3-fold hollow sites, or three different 2-fold bridge sites, or the 6-fold on-top adsorption site, that all have to be realised on a 3-fold substrate (see Fig. 3). Experimentally, for heavy alkali atoms one observes a spin–orbit doublet ($4p_{3/2}$ and $4p_{1/2}$), while the splitting arising from the crystal field is either absent or cannot be resolved in experiments from the Rb 4p shell [51,52]. The atomic model predicts for that case the absence of any CDAD at least for the $p_{1/2}$ state, so that the CDAD observed in experiments is purely of solid state character.

To estimate the influence of the photoelectron diffraction we use a single scattering cluster description (for example see [5,6,24]). Single scattering is the lowest approximations to discuss the most important deviations from the atomic model, but it still gives access to some closed equations that may be used for a direct comparison. However, it is straightforward to include multiple scattering in numerical calculations.

We first restrict the consideration by the nonrelativistic case and neglect all spin effects. As before, we use normal photon incidence with $\boldsymbol{q}\|-\boldsymbol{n}$. The following abbreviations will be used below: $F_j = |f(\vartheta_j)|/(kr_j)\ \sin\{a_j\}\Gamma_j$ is the imaginary part of the scattering amplitude at the jth scattering atom in the cluster. ϑ_j is the scattering angle, r_j is the distance between the emitter and the scattering atom and k is the absolute value of the electron momen-

tum. F_j is corrected for inelastic and thermal processes (Γ_j) and the $1/r_j$ decay of a spherical wave. $a_j = kr_j(1-\cos\ \vartheta_j) + \eta(\vartheta_j)$ is the phase shift, given by the scattering phase η and being corrected for the difference in the path length for the direct and the scattered wave. In the following, s^0 and $d^0 = d^0(k)$ will give the angular parts of the directly emitted partial waves with $l = 0,2$ and $d^j = d^j(k||r_j)$ are the angular parts of the waves scattered at the jth atom (here $\boldsymbol{k}$ and $\boldsymbol{r}_j$ are the unit vectors in the direction of the electron momentum and the position of the scattering atom, respectively). The sums in the following equations have to be taken over all atoms of the cluster. All other quantities are the same as before.

11.1. Non-relativistic case (light alkalis)

We start with the non relativistic (no spin–orbit interaction) expressions that may be used as an example for the photoemission from adsorbed light alkali metals, say the 2p emission from Na. For the three symmetry adapted p states, we find the following equations for the CDAD if using normal photon incidence

b_1, e (p_x) state

$$\frac{I_{\mathrm{CDAD}}(p_x)}{16\pi^2 c_\sigma} = 2\cdot\sqrt{\frac{3}{5}}\cdot s^0 d^0_{xy}\cdot D_s D_d\cdot\sin(\delta_d-\delta_s)\cdot\Gamma_0 - \frac{3}{5}\sum_j\left\{d^0_{xy}\left\{\sqrt{\frac{1}{3}}\,d^j_{z^2}-d^j_{x^2-y^2}\right\} - \left\{\sqrt{\frac{1}{3}}\,d^0_{z^2}-d^0_{x^2-y^2}\right\}d^j_{xy}\right\}\cdot|D_d|^2\cdot F_j \tag{29a}$$

b_2, e (p_y) state

$$\frac{I_{\mathrm{CDAD}}(p_y)}{16\pi^2 c_\sigma} = 2\cdot\sqrt{\frac{3}{5}}\cdot s^0 d^0_{xy}\cdot D_s D_d\cdot\sin(\delta_d-\delta_s)\cdot\Gamma_0 + \frac{3}{5}\sum_j\left\{d^0_{xy}\left\{\sqrt{\frac{1}{3}}\,d^j_{z^2}+d^j_{x^2-y^2}\right\} - \left\{\sqrt{\frac{1}{3}}\,d^0_{z^2}+d^0_{x^2-y^2}\right\}d^j_{xy}\right\}\cdot|D_d|^2\cdot F_j \tag{29b}$$

a_1 (p_z) state

$$\frac{I_{\mathrm{CDAD}}(p_z)}{16\pi^2 c_\sigma} = 0 + \frac{3}{5}\sum_j\{d^0_{yz}d^j_{xz}-d^0_{xz}d^j_{yz}\}\cdot|D_d|^2\cdot F_j \tag{29c}$$

The first line in each equation gives the CDAD expected for the direct emission from the extended atomic model (damped by Γ_0, to ensure that the intensity vanishes in emission parallel to the surface). The most striking result is obtained for the p_z like a_1 state, where even the extended atomic model predicts zero CDAD for normal incidence. We find a CDAD given by the interference of the direct and scattered final state d waves. Similarly we observe a CDAD for the in-plane initial states, even in the degenerate case (3- or 6-fold sites) because only the amount of CDAD emerging from the direct emission is equal and its sign is opposite

e state

$$\frac{I_{\mathrm{CDAD}}(p_{x,y})}{16\pi^2 c_\sigma} = +\frac{6}{5}\sum_j\{d^0_{xy}d^j_{x^2-y^2}\}\cdot|D_d|^2\cdot F_j \tag{29d}$$

It is seen that the scattering induced CDAD is determined only by the interference of waves with the same angular momentum, at least for initial s and p states. In contrast, the atomic like CDAD always depends on the interference of final state partial waves of different orbital angular momentum. This fact may serve to distinguish between both contributions, because scattering induced oscillations will depend much stronger on the kinetic energy through the factor kr in the scattering phase.

Moreover, we will have a remaining CDAD from the direct emission even if the two in-plane levels (b_1, b_2) of a 2-fold bridge site cannot be resolved in an experiment because of the symmetry dependent radial matrix elements (and possibly phases if accounting for the final state symmetry). This fact will change the result obtained from the pure scattering approach. This is not only an effect on the CDAD but also on the observed intensities.

11.2. Relativistic case (heavy alkalis)

Now we would like to compare the emission from the shallow p states of heavy alkali metals (Rb 4p or Cs 5p) in the environment discussed above. In the

case of emission from the p states of heavy alkali atoms, we have to drop the assumption that the spin–orbit interaction can be neglected. Therefore, we have to use the appropriate wave functions from the double group representation. We will first use off-normal photon incidence because the normal incidence CDAD vanishes for all three symmetry adapted p states, as already mentioned above. The CDAD derived from the extended atomic model (that is without including diffraction) is given for an atom in C_{3v} symmetry by the following equations

$e_{1/2}(\mathrm{p}_{1/2})$ state

$$I_{\mathrm{CDAD}}(\mathrm{p}_{1/2}) = 0 \tag{30a}$$

$e_{1/2}(\mathrm{p}_{3/2,1/2})$ state

$$\frac{I_{\mathrm{CDAD}}(\mathrm{p}_{3/2,1/2})}{16\pi^2 c_\sigma} = -(2/5)\cdot \sin a \cdot \sin(2\theta)\cdot \sin(\phi) \cdot f(D,\delta) \tag{30b}$$

$e_{3/2}(\mathrm{p}_{3/2,3/2})$ state

$$\frac{I_{\mathrm{CDAD}}(\mathrm{p}_{3/2,3/2})}{16\pi^2 c_\sigma} = (2/5)\cdot \sin a \cdot \sin(2\theta)\cdot \sin(\phi) \cdot f(D,\delta) \tag{30c}$$

where α is the angle of photon incidence measured as in optics with respect to the surface normal and $f(D,\delta) = 2D_{1/2}[D_{3/2}\ \sin(\delta_{3/2}-\delta_{1/2}) + 4D_{5/2}\ \sin(\delta_{5/2}-\delta_{1/2})] + D_{3/2}D_{5/2}\ \sin\ (\delta_{5/2}-\delta_{3/2})$ contains the dependence on the radial integrals D and phases δ of the different final state channels ($\mathrm{s}_{1/2}$, $\mathrm{d}_{3/2}$ and $\mathrm{d}_{5/2}$). The symmetry and initial state angular momentum indices are omitted for simplicity. The function simplifies to $f(R,\delta) \approx 10 D_{\mathrm{s,p}} D_{\mathrm{d,p}} \sin(\delta_{\mathrm{d}} - \delta_{\mathrm{s}})$ if spin–orbit interaction in the continuum state is neglected. This means that the final state spin–orbit interaction changes the magnitude of the CDAD rather than its angular dependence.

The degeneracy of the p states is removed by the spin–orbit interaction, and the degeneracy of the m_j substates of the $\mathrm{p}_{3/2}$ state is removed by the crystal field. In the atomic model the CDAD for the $\mathrm{p}_{1/2}$ state is identically zero independent of the symmetry or the direction of photon incidence, because it has a spherical charge distribution. The CDAD from the $\mathrm{p}_{3/2}$ state vanishes for normal photon incidence, because both states are aligned along the z axis. For grazing incidence the CDAD vanishes only if a splitting of the $\mathrm{e}_{1/2}$ and $\mathrm{e}_{3/2}$ states is not resolved and the radial matrix elements are independent on the symmetry.

As in the case of the single group consideration, the CDAD becomes modified by photoelectron diffraction. The complete equations become very lengthy if spin-dependent scattering is included. In that case the scattering amplitude F_j has to be replaced by a 2×2 scattering matrix including the spin-flip amplitude [53].

However, only the $\mathrm{d}_{3/2}$ partial wave can be excited in the p→d excitation for an initial $\mathrm{p}_{1/2}$ state. Therefore, it is possible to give a closed equation, at least in a spin independent approximation. Neglecting the spin dependence of the diffraction, we find a simple result for the scattering induced CDAD at normal incidence

$$I_{\mathrm{CDAD}}(\mathrm{p}_{1/2}) \propto \frac{2}{15}\sum_j [\{\mathrm{d}^0_{yz}\mathrm{d}^j_{xz} - \mathrm{d}^0_{xz}\mathrm{d}^j_{yz}\} + 8\{\mathrm{d}^0_{xy}\mathrm{d}^j_{x^2-y^2} - \mathrm{d}^0_{x^2-y^2}\mathrm{d}^j_{xy}\}]\cdot F_j \tag{31}$$

It is seen that the NI-CDAD in emission from the $\mathrm{p}_{1/2}$ state looks the same like the NI-CDAD averaged over all three p states as given in Eq. (29d) for the non relativistic case, what is indeed not surprising.

One may beware of generalising this result. Including all spin effects correctly may change the behaviour as was recently shown in [54] for the Gd surface state. Especially the inclusion of Mott-type scattering will connect, via the spin-flip amplitude, the final state partial waves (e.g. like d_{z^2} and d_{xy}) that are not included in Eq. (31). Therefore, we will illustrate the results later by performing numerical calculations that include all spin effects.

Eq. (31) may also be used to analyse the symmetry properties of the diffraction induced NI-CDAD. We estimate the CDAD from the smallest cluster exhibiting C_{3v} (3-fold hollow) or C_{6v} (on top) symmetry that consists of the adsorbed atom as emitter and the nearest neighbour substrate atoms. The atoms located on the axis of the photon propagation do not contribute to the NI-CDAD as was already shown for emission from s states [34].

Therefore, the atom underneath the emitter in the on-top geometry will not contribute to the CDAD and we have to choose the second nearest neighbours. In the same way it does not matter whether we take an fcc-type or hcp type adsorption site in case of the 3-fold hollow.

For the C_{6v} symmetry we choose the scattering atoms to be located at a distance r from the emitter with $\theta_j = \theta_0$ and $\varphi_j = j^*\pi/3$ ($j = 0 \ldots 5$). We further assume for simplicity that the imaginary part of the scattering amplitude may be reduced to $F_j = \sin\{kr[1 - \cos(\vartheta_j)]\}$ with the scattering angle being $\cos(\vartheta_j) = \sin(\theta)\sin(\theta_0)\cos(\phi - \varphi_j) + \cos(\theta)\cos(\theta_0)$.

Inserting the angular parts into Eq. (31) results in

$$I_{\mathrm{CDAD}}^{C_{6v},\mathrm{p}_{1/2}} \propto \sin(2\theta)\sin(2\theta_0)\sum_j \left[\sin\left(\phi - j\frac{\pi}{3}\right)\right]\cdot F_j(\phi,\varphi_j) + 2\sin^2(\theta)\sin^2(\theta_0)\sum_j \sin\left(2\phi - j\frac{2\pi}{3}\right)\cdot F_j(\phi,\varphi_j) \quad (31a)$$

The scattering amplitude F exhibits the same azimuthal dependence like the remaining φ_j terms determined by the symmetry. In particular the second line will depend on φ_j through $F(\varphi_j)$ and not just on $2\varphi_j$. Therefore, the CDAD will exhibit the symmetry of the adsorption site. We may make some further approximation on F_j to see the azimuthal dependence better. For small kinetic energies and if the emitting atom belongs to the surface or is not too high above the substrate ($z < r$, $\theta_0 \approx \pi/2$) it may reduce further to $F_j \approx kr[1 - \cos\{\sin(\theta)\cos(\phi - j(\pi/3))\}]$. Inserting this approximated value of F_j has the result that the first line vanishes independent of θ and the second for $\theta = 0$. This shows that the CDAD vanishes in normal emission as, expected. However, the symmetry of the adsorption site is reflected in the CDAD through F_j in the second term for off-normal emission. This will not change if we include more atoms in the cluster as far as it still belongs to the C_{6v} symmetry group.

For the C_{3v} symmetry we choose the scattering atoms to be located at $\theta_j = \theta_0$ and $\varphi_j = j^*2\pi/3$ ($j = 0 \ldots 2$). After inserting the angular parts, we will find that the symmetry of the 3-fold hollow is reflected as it was in the case of the on top site. From Fig. 3 we have seen that there are two different 3-fold hollows available, an upward and a downward oriented triangle. These two situations are realised by adding an offset $\varphi_0 = \pm\pi/2$ to the azimuthal angle φ_j of the substrate positions. This results in

$$\begin{aligned} I_{\mathrm{CDAD}}^{C_{3v},\mathrm{p}_{1/2}} \propto{}& \sin(2\theta)\sin(2\theta_0)\sum_j \sin\left(\phi - j\frac{2\pi}{3} \mp \frac{\pi}{2}\right)\cdot F_j(\phi,\varphi_j) + 2\sin^2(\theta)\sin^2(\theta_0)\cdot\sum_j \sin\left(2\phi - j\frac{4\pi}{3} \mp \pi\right)\cdot F_j(\phi,\varphi_j) \\ ={}& \sin(2\theta)\sin(2\theta_0)\sum_j \mp\cos\left(\phi - j\frac{2\pi}{3}\right)\cdot F_j\left[\mp\cos\left(\phi - j\frac{2\pi}{3}\right)\right] - 2\sin^2(\theta)\sin^2(\theta_0)\sum_j \sin\left(2\phi - j\frac{4\pi}{3}\right)\cdot F_j\left[\mp\cos\left(\phi - j\frac{2\pi}{3}\right)\right] \end{aligned} \quad (31b)$$

The CDAD of each domain will show separately a 3-fold symmetry as can be seen by a comparison to the C_{6v} discussion. If not resolved, one has to average over both domains. Now, one finds that the first term vanishes if we add the CDAD from both C_{3v} hollow sites, whereas the sum of the second term will show a 6-fold symmetry. This second term may vanish for particular values of the polar angles. Anyway, the CDAD from the superposition of the two equivalent C_{3v} adsorption sites results always in a pseudo-C_{6v} symmetry independent of particular choices for F_j.

11.3. Numerical calculation for heavy alkali metals

Above we gave a very simplified approximation. We neglected in the discussion of (26a) and (26b) the role of the scattering amplitude. In the following, we will present numerical results obtained for the p state emission. The restrictions as used to derive the closed (single scattering) equations do not apply to the numerical calculations. The calculations were performed within a 2-step model as described previously [24,29,54]. The calculations are fully relativistic, accounting for spin–orbit interaction in the initial and final atomic states as well as in scattering. We have chosen the geometrical parameter of the

Pt(111)−($\sqrt{3}\times\sqrt{3}$)R30°–Rb structure for illustration ($d_{\mathrm{Pt-Pt}}=2.77$ Å, $d_{\mathrm{Rb-Rb}}=\sqrt{3}\ d_{\mathrm{Pt-Pt}}\approx 4.8$ Å, $d_{\mathrm{Rb-Pt}}=3.78$ Å). The initial state was assumed to be the shallow 4p core level of the Rb adsorbate. The kinetic energy of the photoelectrons was set to 30 eV ($k=2.8$ Å^{-1}). The use of higher kinetic energies will force more oscillations in the azimuthal dependence. This will make the result rather confusing without bringing more insight into the symmetry properties. An electron mean free path of about 7 Å was assumed. To avoid problems arising from slightly different number of atoms in the clusters with different symmetry and to have a better comparison we use the asymmetry defined by:

$$A_{\mathrm{CDAD}}=\frac{I^{\mathrm{RCP}}-I^{\mathrm{LCP}}}{I^{\mathrm{RCP}}+I^{\mathrm{LCP}}}. \tag{37}$$

We start with a calculation for the Rb $4p_{1/2}$ state. Fig. 4 compares the CDAD for the 6-fold on top and the two superimposed 3-fold hollow sites depending on the azimuthal angle at a fixed polar angle $\theta=45°$. A maximum CDAD asymmetry of about 4% is obtained in case of the on top site, whereas it is about three times higher for the hollow site. These values are due to the particular polar angle used here.

The most interesting result is that we find a 6-fold pattern for both the on-top site and the superimposed hollow sites. Apparently, neither the calculation for the on-top nor that for the 3-fold hollow adsorption site reflects the 3-fold structure of the fcc Pt(111) substrate but only a 6-fold symmetry. The superposition of the CDAD from the hollow sites averages not only over the two possible 3-fold adsorption sites but also over the 3-fold symmetry of the substrate. These symmetry properties do not change in the case of the $4p_{3/2}$ state independent whether the crystal field splitting is resolved or not, as was checked by calculations for those states. This demonstrates that the most simple approximation as given above by the closed equations is sufficient to explain the basic symmetry properties of the CDAD.

The result for the hollow site shows that the local 3-fold symmetry is completely lost but a pseudo 6-fold symmetry is observed if the domains are not distinguishable. Therefore, we treated the domains

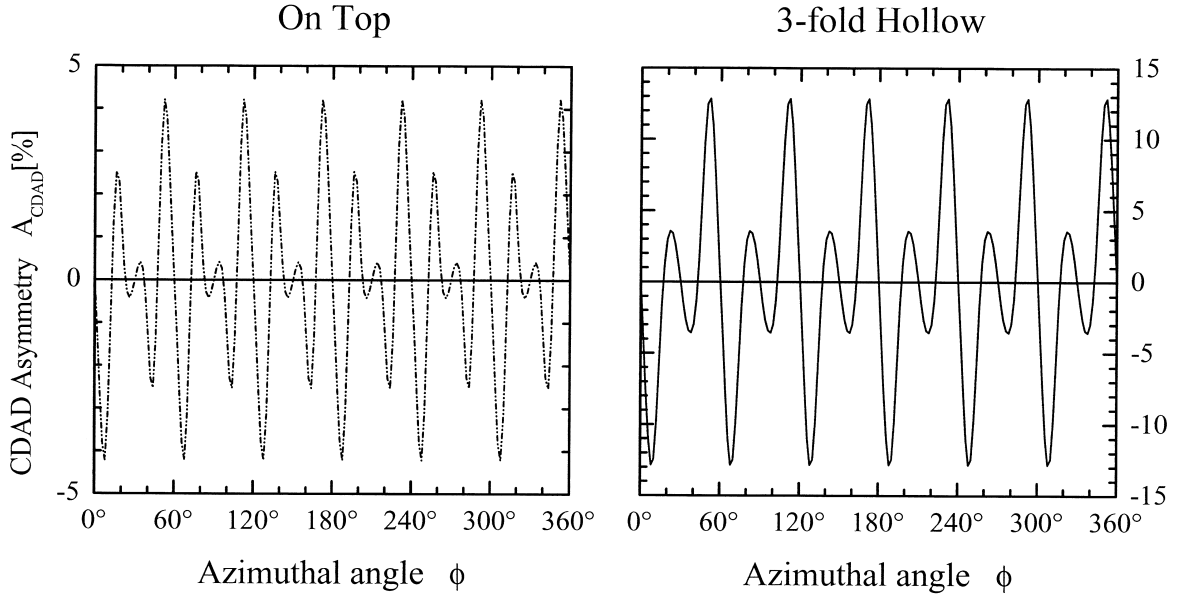

Fig. 4. Domain averaged CDAD from the Rb $4p_{1/2}$ shell: Pt(111)–($\sqrt{3}\times\sqrt{3}$)–R30°–Rb comparing on-top-site (left) and 3-fold hollow site adsorption (right). The 3-fold hollow site calculation is averaged over the two possible domains that are shown in Fig. 3 as well as the possible stacking orders of the substrate. The calculations are for a kinetic energy of $E_{\mathrm{kin}}=30$ eV; a polar angle of $\theta=45°$ and normal photon incidence.

separately and received the results shown in Fig. 5 for the $4p_{3/2}$ derived CDAD. Now, the local 3-fold symmetry is reflected by all states, even if the $e_{1/2}$ and $e_{3/2}$ states are not resolved. Obviously, the domain resolved CDAD has much higher values compared to the domain averaged one. Moreover, it is seen that the extrema of the two different sites are shifted by 90°, as expected from the discussion of the closed equations.

As we have shown, not the absolute square of quantities describing the photoemission but the complex amplitudes themselves enter the scattering part, which is independent of the kind of solid state calculations (single or 3-step) used. Therefore, we like to hint that most of the previously published work using purely atomic models is not directly applicable to describe angular resolved core level photoemission from solids or adsorbates if only the final, most often integrated, results are given instead of the wave functions or say better their complex amplitudes. Nevertheless, the wave functions derived from the atomic models are still very useful to be used in the initial step of 2- or 3-step calculations. The inclusion of magnetic and many-electron effects using such symmetry adapted wave functions will be part of future work.

The large differences in the CDAD show that it may be possible to detect the two domains separ-

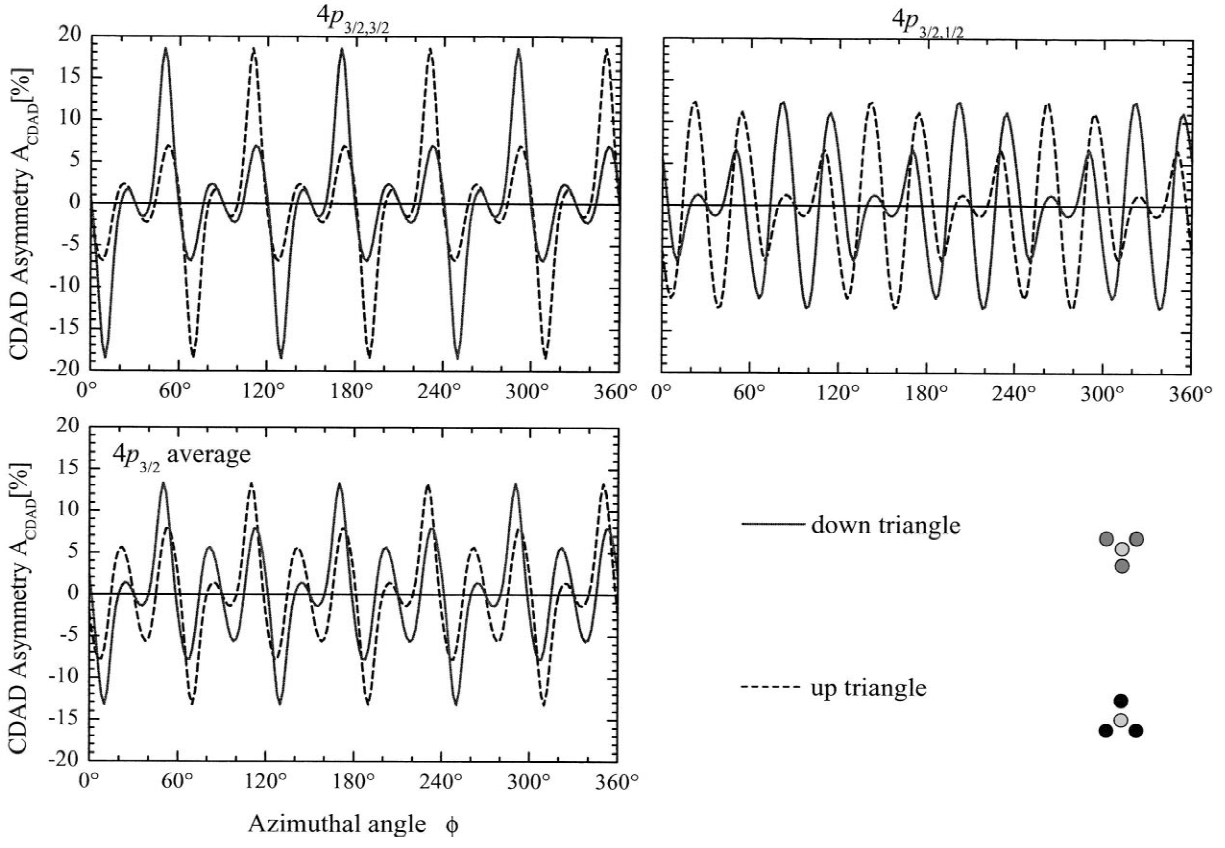

Fig. 5. Domain resolved CDAD from the Rb-4p shell: Pt(111)–($\sqrt{3}\times\sqrt{3}$)–R30°–Rb for 3-fold hollow site adsorption. The upper row shows the CDAD for the two crystal field split Rb $4p_{3/2}$ states with $|m_j|=1/2$ or $3/2$. The lower left graph shows the CDAD for the average of the two $|m_j|$ substates of the $4p_{3/2}$ state for cases where the crystal field splitting is not resolved. Dashed and dotted lines are for the two possible geometrical arrangements that are rotated by 180° with respect to each other, resulting either in up or in down triangles (see Fig. 3). The calculations are for a kinetic energy of $E_{kin}=30$ eV; a polar angle of $\theta=45°$ and normal photon incidence.

ately, if we have an experimental method to investigate the structure with high spatial resolution. A particular orientation of the 3-fold hollow site in an ordered overlayer can only be realised in a domain of several adsorbed atoms rather than for a single atom. Such domains are naturally sized as large as the transfer width of LEED (low energy electron diffraction) at least, otherwise no ordered pattern is observed. It was recently shown in [34] that circular dichroism from adsorbed molecules can be measured with high lateral resolution (sub μm range) by means of photoemission electron microscopy (PEEM) [55,56]. Similarly one may use instruments like a scanning X-PEEM (see Part III in [57] and references therein), provided one has a focused source for circularly polarised X-rays. The only necessary condition to resolve the domains by means of CDAD is that the domains belonging to the different structures are large enough to be resolved by the instrument. The strong differences in the azimuthal dependence may serve to distinguish easily the different domains by measuring the CDAD at a single polar and azimuthal angle.

12. Summary and conclusions

In the past, most of the CDAD experiments have been done for off-normal photon incidence. One reason is that the usual atomic or molecular models predicted the absence of CDAD for normal incidence that is along the principal axis of symmetry. This may also be the reason that possibly in some experiments the occurrence of CDAD was overlooked or effects of the circularly polarised photons were interpreted incompletely.

To overcome this misinterpretation regarding the CDAD, we presented an extension of the atomic model for consideration of photoionization from non-ferromagnetic solids and adsorbed atoms. The CDAD was theoretically investigated for atoms in C_{nv} symmetry ($n=2,..,6$) with a special emphasis on the case of photon propagation antiparallel to the principal axis of the atoms. An extension to all other symmetry groups is straightforward if using compatibility relations between the basic states of different irreducible representations. It is shown that the normal incidence CDAD is different from zero in the extended model for photoionization of closed shells, in contrast to an ensemble of axially symmetric aligned atoms.

We found that the normal incidence CDAD reflects the symmetry of the adsorption site or the symmetry of the surface for particular cases of *l*. For atoms with C_{2v} symmetry, the azimuthal dependence of the CDAD enables a distinction to be made between the photoionization of *a* states sin (4ϕ) oscillations in the NI-CDAD and the *b* states [sin (2ϕ)]. For atoms with C_{4v} (d shell) and C_{6v} symmetry (f shell) we found sin (4ϕ) and sin (6ϕ) oscillations, respectively. We have also shown the occurrence of a CDAD in d shell ionisation respecting incidence along one of the principal axes of the O_h group. It exhibits sin (4ϕ) oscillations for the degenerate e_g or t_{2g} states. The D_{6h} symmetry group needs at least $l=3$ initial states for the occurrence of an NI-CDAD. Inclusion of the coupling of states by the crystal field potential shows that the CDAD from the states of the double groups will also exhibit the symmetry of the adsorption site or solid environment.

The NI-CDAD reflects the symmetry of the initial states in all cases investigated. The non-zero CDAD results here from the distortion of the spherical symmetry in the initial states of adsorbates or atoms in a solid. Besides that, the final state symmetry and scattering of the photoelectrons from the surrounding atoms will also contribute to the CDAD. The different contributions may be separated experimentally by energy and angular dependent measurements.

Finally, we have shown for a particular adsorbate structure (C_{3v} and C_{6v} symmetry) that the atomic model breaks completely down for p-states and the states of the double groups. It is not able to describe the circular dichroism in the angular distribution if comparing it to calculations respecting the full solid environment. Electron scattering effects strongly the angular distributions independent of the initial state. In most cases it will dominate the structures of the angular distribution.

Acknowledgements

This research was supported by a joint grant of the Deutsche Forschungsgemeinschaft (grant no. 436

RUS 113/372) and the Russian Fund for Basic Research (grant no. 96-02-00155G) and by Sonderforschungbereich 262. V.V.K and N.A.C are grateful for the hospitality of the Johannes Gutenberg-Universität Mainz extended to them during the work on this paper.

References

[1] H. Daimon, T. Nakatani, S. Imada, S. Suga, Y. Kagoshima, T. Miyahara, Jpn. J. Appl. Phys. 32 (1993) L1480;
H. Daimon, T. Nakatani, S. Imada, S. Suga, J. Elect. Spectros. Rel. Phenom. 76 (1995) 55.
[2] C.S. Fadley, Surf. Sci. Rep. 19 (1993) 231.
[3] R. Feder, in: R. Feder (Ed.), Polarized Electrons in Surface Physics, World Scientific, 1985.
[4] J. Braun, Rep. Prog. Phys. 59 (1996) 1267.
[5] C.S. Fadley, in: R.Z. Bacharach (Ed.), Synchrotron Radiation Research, Vol. 1, Plenum Press, New York, 1992.
[6] D.P. Woodruff, A.M. Bradshaw, Rep. Prog. Phys. 57 (1994) 1029.
[7] J.B. Pendry, Surf. Sci. 57 (1976) 679.
[8] C.S. Fadley, in: C.R. Brundle, A.D. Baker (Eds.), Electron Spectroscopy: Theory Techniques and Applications, Vol. 2, Academic Press, London, 1978.
[9] N.A. Cherepkov, V.V. Kuznetsov, J. Phys.: Condens. Matter 8 (1996) 4971.
[10] D. Venus, Phys. Rev. B 49 (1994) 8821.
[11] B.T. Thol, G. van der Laan, Phys. Rev. B 44 (1991) 12424;
B.T. Thol, G. van der Laan, Phys. Rev. Lett. 70 (1993) 2499;
B.T. Thol, G. van der Laan, Phys. Rev. B 49 (1994) 9613;
B.T. Thol, G. van der Laan, Phys. Rev. B 50 (1994) 11474.
[12] S.Y. Tong, X. Guo, J.G. Tobin, G.D. Waddill, Phys. Rev. B 54 (1996) 15356.
[13] A. Liebsch, Phys. Rev. Lett. 32 (1974) 1203;
A. Liebsch, Phys. Rev. B 13 (1976) 544.
[14] J.W. Gadzuk, Phys. Rev. B 12 (1975) 5608.
[15] J.F. Herbst, Phys. Rev. B 15 (1977) 3720.
[16] S.M. Goldberg, C.S. Fadley, S. Kono, J. Elect. Spectros. Rel. Phenom. 21 (1981) 285.
[17] G. Schönhense, Phys. Script. T31 (1990) 255;
G. Schönhense, Vacuum 41 (1990) 506.
[18] J. Bansmann, Ch. Ostertag, M. Getzlaff, G. Schönhense, N.A. Cherepkov, V.V. Kusnesov, A.A. Pachlichev, Z. Phys. D 33 (1995) 257.
[19] B. Ritchie, Phys. Rev. A 12 (1975) 567;
B. Ritchie, Phys. Rev. A 13 (1976) 1411;
B. Ritchie, Phys. Rev. A 14 (1976) 359.
[20] R. Feder, Solid State Comm. 21 (1977) 1091.
[21] R. Parzynski, Acta Phys. Pol. A 57 (1980) 49.
[22] N.A. Cherepkov, Chem. Phys. Lett. 87 (1982) 344.
[23] R.L. Dubs, S.N. Dixit, V. McKoy, Phys. Rev. Lett. 54 (1985) 1249;
R.L. Dubs, S.N. Dixit, V. McKoy, Phys. Rev. B 32 (1985) 8389.
[24] G.H. Fecher, Europhys. Lett. 29 (1995) 605.
[25] N.A. Cherepkov, Sov. Phys. JETP 38 (1974) 463;
N.A. Cherepkov, Phys. Rev. B 50 (1994) 13813.
[26] G. van der Laan, Phys. Rev. B 51 (1995) 240;
G. van der Laan, Phys. Rev. B 55 (1997) 3656.
[27] H. Klar, H. Kleinpoppen, J. Phys. B 15 (1982) 933.
[28] C. Westphal, A.P. Kaduwela, C.S. Fadley, M.A. van Hove, Phys. Rev. B 50 (1994) 6203.
[29] G.H. Fecher, A. Oelsner, Ch. Ostertag, G. Schönhense, J. Elect. Spectros. Rel. Phenom. 76 (1995) 97.
[30] A.P. Kaduwela, H. Xiao, S. Thevuthasan, C.S. Fadley, M.A. van Hove, Phys. Rev. B 52 (1995) 14927.
[31] M.A. van Hove, A.P. Kaduwela, H. Xiao, W. Schattke, C.S. Fadley, J. Elect. Spectros. Rel. Phenom. 80 (1996) 137.
[32] A. Chasse, P. Rennert, J. Elect. Spectros. Rel. Phenom. 87 (1997) 91;
A. Chasse, P. Rennert, J. Phys. Chem. Solids 58 (1997) 509.
[33] A. Oelsner, G.H. Fecher, J. Electr. Spectr. Rel. Phen. 101–103 (1999) 445.
[34] G.H. Fecher, Jpn. J. Appl. Phys. 38 (1999) S582.
[35] R.X. Ynzunza, H. Daimon, F.J. Palomares, E.D. Tober, Z. Wang, F.J. Garcya de Abajo, J. Morais, R. Denecke, J.B. Kortright, Z. Hussain, M.A. van Hove, C.S. Fadley, J. Elect. Spectros. Rel. Phenom. 106 (2000) 7.
[36] N.A. Cherepkov, V.V. Kuznetsov, J. Phys. B 22 (1989) L405.
[37] N.A. Cherepkov, V.V. Kuznetsov, V.A. Verbitskii, J. Phys. B 28 (1995) 1221.
[38] K. Blum, Density Matrix Theory and Application, Plenum, New York, 1981.
[39] G.H. Fecher, J. Elect. Spectros. Rel. Phenom. 114–116 (2001) 1165.
[40] J.E. Inglesfield, B.W. Holland;, in: D.A. King, D.P. Woodruf; (Eds.), The Chemical Physics of Solid Surfaces and Heterogeneous Catalysis, Elsevier, Amsterdam, 1981, p. 183.
[41] E.U. Condon, G.H. Shortley, The Theory of Atomic Spectra, Cambridge University Press, London, 1977;
S.L. Altmann, Proc. Camb. Phil. Soc. 53 (1957) 343;
S.L. Altmann, C.J. Bradley, Phil. Trans. R. Soc. A 255 (1963) 199.
[42] W. Ludwig, C. Falter, Symmetries in physics, in: Springer Series in Solid-state Science, Vol. 64, Springer-Verlag, Berlin, 1988.
[43] D.C. Harris, M.D. Bertolucci, Symmetry and Spectroscopy, Dover, New York, 1989.
[44] D. Venus, W. Kuch, A. Dittschar, M. Zharnikov, C.M. Schneider, J. Kirschner, Phys. Rev. B 52 (1995) 6174.
[45] J.C. Slater, G.F. Koster, Phys. Rev. 94 (1954) 1948.
[46] T. Matsushita, S. Imada, H. Daimon, T. Okuda, K. Yamaguchi, H. Miyagi, S. Suga, Phys. Rev. B 56 (1997) 7687.
[47] J. Hölzl, F.K. Schulte, Solid surface physics, in: Springer Tracts in Modern Physics, Vol. 85, 1979;
J. Hölzl, L. Fritsche, Surf. Sci. 247 (1991) 226.
[48] E. Wimmer, A.J. Freeman, J.R. Hiskers, A.M. Karo, Phys. Rev. B 28 (1983) 3074.

[49] Y. Onodera, M. Okazaki, J. Phys. Soc. Jpn. 21 (1966) 2400.
[50] J. Meyer, W.-D. Sepp, B. Fricke, A. Rosen, Comp. Phys. Commun. 96 (1996) 263.
[51] A. Oelsner, G.H. Fecher, Ch. Ostertag, Th. Jentzsch, G. Schönhense, Surf. Sci. 331–333 (1995) 349.
[52] G.H. Fecher, J. Bansmann, C. Grünewald, A. Oelsner, C. Ostertag, G. Schönhense, Surf. Sci. 307–309 (1994) 70; G.H. Fecher, A. Oelsner, Ch. Ostertag, G. Schönhense, J. Electr. Spectr. Rel. Phenom. 76 (1995) 289.
[53] J. Kessler, Polarized electrons, in: 2nd Edition, Springer Series On Atoms and Plasmas, Vol. 1, Springer, Berlin, 1985.
[54] N.A. Cherepkov, G.H. Fecher, Phys. Rev. B 61 (2000) 2561.
[55] W. Swiech, G.H. Fecher, Ch. Ziethen, O. Schmidt, G. Schönhense, K. Grzelakowski, C.M. Schneider, R. Frömter, H.P. Oepen, J. Kirschner, J. Electr. Spectr. Rel. Phenom. 84 (1997) 171.
[56] E. Bauer, J. Electr. Spectr. Rel. Phenom. 114–116 (2001) 975.
[57] J. Thieme, G. Schmahl, D. Rudolph, E. Umbach (Eds.), X-ray Microscopy and Spectroscopy, Springer, Berlin, 1998.